SEL1L degradation intermediates stimulate cytosolic aggregation of polyglutamine-expanded protein

Tokuya Hattori [1], Ken Hanafusa [1], Ikuo Wada [2], Nobuko Hosokawa[1]

[1] Department of Molecular and Cellular Biology, Institute for Frontier Medical Sciences, Kyoto University, Kyoto 606-8397, Japan

[2] Department of Cell Science, Institute of Biomedical Sciences, Fukushima Medical University School of Medicine, Fukushima 960-1295, Japan

Running title: *SEL1L degradation stimulates polyQ aggregation*

Correspondence: Nobuko Hosokawa, Laboratory of Molecular and Cellular Biology, Institute for Frontier Medical Sciences, Kyoto University, 53 Kawahara-cho, Sakyo-ku, Kyoto City, Kyoto 606-8507, Japan; Tel.: +81-75-751-3849; Fax: +81-75-751-4646; E-mail: nobukoh@infront.kyoto-u.ac.jp

Abbreviations: α_1AT, α_1-antitrypsin; ER, endoplasmic reticulum; ERAD, ER-associated

degradation; GFP, green fluorescent protein; Htt, Huntingtin; NP-40, Nonidet P-40; polyQ, poly-glutamine; SLR, SEL1-like repeat

Keywords: ER-associated degradation (ERAD); HRD1-SEL1L ubiquitin ligase complex; OS-9; polyQ aggregation; XTP3-B

Abstract

Misfolded proteins in the endoplasmic reticulum (ER) are degraded by ER-associated degradation (ERAD). In mammalian cells, the HRD1–SEL1L membrane ubiquitin ligase complex plays a central role in this process. However, SEL1L is inherently unstable, and excess SEL1L is also degraded by ERAD. Accordingly, when proteasome activity is inhibited, multiple degradation intermediates of SEL1L appear in the cytosol. In this study, we searched for factors that inhibit SEL1L degradation, and identified OS-9 and XTP3-B, two ER lectins that regulate glycoprotein ERAD. SEL1L degradation was characterized by a ladder of degradation products, and the C-terminal Pro-rich region of SEL1L was responsible for generation of this pattern. In the cytosol, these degradation intermediates stimulated aggregation of polyglutamine-expanded Huntingtin protein (Htt-polyQ-GFP) by interacting with aggregation-prone proteins, including Htt-polyQ-GFP. Collectively, our findings indicate that peptide fragments of ER proteins generated during ERAD may affect protein aggregation in the cytosol, revealing the interconnection of protein homeostasis across subcellular compartments.

Introduction

Large quantities of secretory and membrane proteins are synthesized in the endoplasmic reticulum (ER). Protein quality control mechanisms strictly regulate the folding of newly synthesized proteins to ensure their efficient production and transport through the secretory pathway [1, 2]. However, some protein misfolding is inevitable, and the resultant aberrant conformers must be cleared to prevent adverse interactions with other polypeptides. Many misfolded secretory proteins are retrotranslocated from the ER to the cytosol for degradation by the proteasome, a mechanism known as ER-associated protein degradation (ERAD) [3, 4]. This system, which is conserved across the eukaryotes, relies on a ubiquitin ligase in the ER membrane. In *S. cerevisiae*, Hrd1 is the ubiquitin ligase required for degradation of ERAD substrates with misfolded domains in the ER lumen (ERAD-L) or misfolding in the membrane region (ERAD-M) [5]. Hrd1 forms a stoichiometric complex with Hrd3, which is required for degradation of ERAD-L substrates. Several molecules, including the pseudorhomboid protein Der1, the ER lectin Yos9, the transmembrane protein Usa1, and the AAA ATPase Cdc48, associate and collaborate with the Hrd1–Hrd3 ubiquitin ligase complex to achieve retrotranslocation. A recent structural analysis using cryoelectron microscopy revealed that Hrd1 forms a half-channel on the cytosolic side of the retrotranslocation machinery for ERAD-L substrates [6].

Mammals have two homologs of Hrd1, HRD1 and gp78/synoviolin. Of the two, only HRD1 forms a stable complex with SEL1L, the homolog of yeast Hrd3. Additionally, mammals have three homologs of Der1, Derlin-1, -2, and -3, and two homologs of Yos9, OS-9 and XTP3-B [4, 7]. The components of the retrotranslocation machinery assembled around the Hrd1–Hrd3 ubiquitin ligase complex in yeast appears to be conserved in mammals; however, the exact composition of the mammalian retrotranslocon remains to be elucidated.

Imbalances of protein homeostasis result in protein aggregation, which in turn causes several human diseases [8-10]. Expansion of polyglutamine tracts generates aggregates, leading to neurodegenerative diseases including Huntington's disease and spinocerebellar ataxia [11, 12]. PolyQ inclusions form in the neurons of patients and mouse models, as well as in cultured mammalian and yeast cells. Furthermore, protein homeostasis is tightly regulated among subcellular compartments, including the ER and cytosol; consequently, polyQ aggregation in the cytosol impairs ERAD and causes ER stress [13].

Recently, we showed that human SEL1L is inherently unstable unless in a membrane complex with HRD1, and that the transmembrane region of SEL1L is responsible for its instability [14]. Interestingly, we noticed that SEL1L degradation intermediates accumulate when proteasome activity is inhibited [15]. Most ERAD substrates are degraded immediately after extraction from the ER, and such degradation intermediates are usually not detected even in the

presence of proteasome inhibitors. Hence, we further characterized the SEL1L degradation process and confirmed that after translocation into the ER, SEL1L is extracted and degraded in the cytosol. In addition to HRD1, we found that the ER lectins OS-9 and XTP3-B also stabilize SEL1L. Interestingly, accumulation of these degradation intermediates in the cytosol stimulated the cytosolic aggregation of polyglutamine-expanded Htt protein, probably through the interaction of SEL1L-like repeats (SLR) with aggregation-prone proteins in the cytosol, implying that SEL1L has an intrinsic chaperone-like property.

Results

SEL1L degradation intermediates can be detected upon inhibition of proteasome activity

In a previous study, we revealed that SEL1L is a short-lived protein that is rapidly degraded by the proteasome in the absence of HRD1 [15]. When proteasome activity was inhibited, we detected accumulation of SEL1L degradation intermediates of various sizes. However, because such intermediates are not commonly detected during the proteasomal degradation of ERAD substrates, we further characterized the degradation mechanism of SEL1L. Human SEL1L is a type I transmembrane protein containing eleven SLRs (Fig. 1A) [16]. We expressed wild-type SEL1L, C-terminally HA-tagged SEL1L (SEL1L-HA) [14], and N-terminally S-tagged SEL1L (S-SEL1L) [17] in HEK 293 cells and analyzed the proteins by Western blotting. However, the expression levels of the full-length SEL1L proteins were not increased, which is consistent with our previous reports [14, 15]. Instead, anti-SEL1L antibody, which reacts with the C-terminal 15 amino acids of SEL1L protein, recognized several fragments in cells overexpressing WT SEL1L, SEL1L-HA, or S-SEL1L when proteasome activity was inhibited (Fig. 1B, MG132 +, indicated by angle brackets). The fragments had the same electrophoretic mobilities in cells overexpressing WT SEL1L and S-SEL1L (Fig. 1B, lanes 4 and 8), and migrated slightly more slowly in cells expressing SEL1L-HA due to the HA-tag at the C-terminus (Fig. 1B, lane 6). Anti–S-tag antibody

recognized several fragments in addition to full-length S-SEL1L (Figure 1B, Blot S-tag, lane 12). In cells expressing SEL1L-HA, anti-HA antibody detected the same fragments as the SEL1L antibody (Fig. 1B, Blot HA, lane 16). Together, these results indicate that both the N- and C-terminal portions of SEL1L were cleaved when proteasome activity was inhibited.

We next transfected FolA-S-HA, in which the SEL1L luminal domain was replaced by the bacterial FolA (DHFR) protein [14]; hence, FolA-S-HA contains the transmembrane and cytosolic domains of SEL1L. Consistent with our previous findings that the transmembrane region of SEL1L is responsible for its instability [14], degradation intermediates of the chimeric protein were detected in the presence of MG132 (Fig. 1C).

To analyze the ubiquitination of these SEL1L degradation intermediates, we co-transfected wild-type SEL1L and HA-ubiquitin and immunoprecipitated full-length and truncated SEL1L with anti-SEL1L antibody. Blotting with anti-HA-tag antibody revealed a smear of slowly migrating bands in cells treated with MG132 (Fig. 1D, lane 8), indicating that the SEL1L degradation intermediates were ubiquitinated. HA-ubiquitin signals were also detected below the 50 kDa molecular weight marker, indicating that SEL1L degradation intermediates of lower molecular weights were also ubiquitinated.

Next, we analyzed the stability of transfected S-SEL1L by pulse-chase experiments (Fig. 1E). Rapid degradation of S-SEL1L was strongly inhibited in the presence of MG132; this observation

was confirmed using both antibodies against the N-terminal S-tag and C-terminal SEL1L (Fig. 1E, quantified in the graph). S-SEL1L degradation intermediates were also detected. Collectively, these results suggest that restricted cleavage of SEL1L occurs during ERAD.

SEL1L degradation intermediates are located in the cytosol

To determine whether SEL1L degradation intermediates are generated in the ER or the cytosol, we investigated the intracellular localization of these peptides. HEK 293 cells expressing control plasmid, SEL1L-HA, or S-SEL1L were fractionated into cytosolic (CE), membrane (containing the ER) (ME), and nuclear extracts (NE) using Subcellular Fractionation Kit (Fig. 2A–C). SEL1L fragments were mainly detected in CE (Fig. 2A, lanes 10 and 16; Fig. 2B, lane 10), whereas full-length SEL1L-HA and S-SEL1L were mainly in the ME (Fig. 2A, lanes 11 and 17; Fig. 2B, lane 11). The integrity of each fraction was validated by immunoblotting for ER marker protein (calnexin) and cytosolic proteins (actin and HSC70/HSP70) (Fig. 2C).

The subcellular localization of SEL1L degradation intermediates was further analyzed by another subcellular fractionation procedure without using detergents (Fig. 2D, E). Cell homogenates prepared by passing cells through a 30-G needle were separated into cytosol (S: 100 k × g supernatant) and microsome (P: 100 k × g pellet) fractions by ultracentrifugation at 100,000 × g. SEL1L degradation intermediates were clearly detected in the cytosolic fractions (Fig. 2D,

lanes 7 and 11; Fig. 2E, lane 7). Collectively, these results indicate that SEL1L degradation intermediates accumulate in the cytosol.

SEL1L degradation intermediates are generated in the cytoplasm after retrotranslocation

Mature SEL1L contains eight Cys residues, some of which form disulfide bonds (Fig. 1A). Accordingly, the electrophoretic mobility of endogenous SEL1L in SDS-PAGE was slower under non-reducing conditions than under reducing conditions (Fig. 3A, compare lanes 1 and 5). Similarly, transfected full-length WT SEL1L, S-SEL1L, and SEL1L-HA migrated more slowly under non-reducing conditions (Fig. 3A, arrows, compare lanes 2–4 with 6–8), indicating that full-length SEL1L protein was disulfide-bonded and expressed in the ER. On the other hand, the electrophoretic mobilities of SEL1L fragments were similar on reducing and non-reducing gels (Fig. 3A, angle brackets, compare lanes 2–4 with 6–8), indicating that these fragments lacked disulfide bridges and localized in a reducing milieu, probably the cytoplasm. We then compared the electrophoretic mobilities of SEL1L degradation intermediates with those of cytosolically expressed SEL1L. SEL1L-HA lacking the signal sequence (ΔssSEL1L-HA) was rapidly degraded, and degradation intermediates were detected when proteasome activity was inhibited (Fig. 3B, lanes 3, 4). The electrophoretic mobilities of the fragments originating from SEL1L-HA and ΔssSEL1L-HA were almost identical (Fig. 3B, compare lanes 2 and 3), further supporting the idea

that SEL1L degradation intermediates were generated in the cytosol. These results suggest that SEL1L was initially sequestered in the ER lumen, and that the degradation intermediates were generated in the cytosol immediately after extraction from the ER.

A pre-emptive quality control mechanism mitigates ER protein overload by inhibiting the translocation of ER proteins, resulting in expression of these proteins in the cytosol for degradation [18]. To confirm that the SEL1L degradation intermediates originated from SEL1L expressed in the ER, and not from SEL1L protein that failed to enter the ER during translation, we treated cells with the PNGase inhibitor Z-VAD-FMK [19]. SEL1L has five potential N-glycosylation sites; during the ERAD process, N-glycans are removed from glycoproteins by the cytoplasmic PNGase [20]. The electrophoretic mobility of SEL1L fragments was slower in cells treated with PNGase inhibitor (Fig. 3C, compare lanes 3 and 4, black and red angle brackets), indicating that these fragments were generated from N-glycosylated SEL1L proteins. Removal of N-glycans from the glycoprotein converts Asn residues to Asp, resulting in a change in the protein's isoelectric point [21]. To confirm that SEL1L-HA degradation intermediates were deglycosylated by the cytosolic PNGase, we compared the isoelectric points of SEL1L fragments with those of cytosolically expressed ΔssSEL1L-HA fragments by IEF-SDS-PAGE (Fig. 3D). SEL1L degradation intermediates had more acidic isoelectric points than those generated from ΔssSEL1L-HA (Fig. 3D, compare red and black arrows), confirming that SEL1L degradation

intermediates are deglycosylated.

Extraction of ERAD substrates from the ER requires the AAA+ ATPase p97/VCP [22]. In cells overexpressing SEL1L-HA, degradation intermediates disappeared upon addition of MNS-873, a p97/VCP inhibitor [23] (Fig. 3E, lane 4), further confirming that p97-dependent extraction precedes SEL1L degradation.

OS-9 and XTP3-B inhibits the degradation of SEL1L

The HRD1–SEL1L ubiquitin ligase complex forms a large assembly in the ER membrane that contains multiple factors involved in ERAD [4, 7]. Hence, we co-transfected cells with proteins that specifically interact with SEL1L and analyzed the effect on generation of SEL1L degradation intermediates. OS-9 and XTP3-B are ER lectins that recognize misfolded glycoproteins destined for ERAD [24]. Co-expression of OS-9 or XTP3-B inhibited S-SEL1L degradation, whereas co-transfection of NHK-QQQ, a typical ERAD substrate that binds to SEL1L, did not (Fig. 4A, B). We then analyzed the effect of other ER proteins that might interact with SEL1L. Co-expression of BiP, PDI-FLAG, or EDEM3-HA did not inhibit accumulation of SEL1L degradation intermediates (Fig. 4C). As expected, Calnexin-HA, which assists in glycoprotein maturation and does not interact with the ERAD membrane complex, did not affect generation of SEL1L fragments (Fig. 4C).

We then analyzed the effect of depleting endogenous OS-9 and XTP3-B on the expression of endogenous SEL1L. siRNA-mediated knockdown of OS-9 moderately inhibited the expression of SEL1L, whereas knockdown of XTP3-B had no such effect (Fig. 4D, quantified in E). Interestingly, silencing of both OS-9 and XTP3-B decreased SEL1L expression (Fig. 4D, E). In addition, knockdown of XTP3-B increased the expression of OS-9 (Fig. 4D, quantified in F), whereas depletion of OS-9 did not affect the level of XTP3-B (Fig. 4D, quantified in G). Given that increased expression of OS-9 stabilized SEL1L (Fig. 4A), these results suggest that either OS-9 or XTP3-B is required to stabilize SEL1L.

Regulation of the stability of the HRD1–SEL1L complex is important for disposal of misfolded cargo proteins, and transient expression of SEL1L promotes ERAD of terminally misfolded NHK-QQQ (Fig. 4H, compare lanes 1–3 and 4–6) [14, 15]. However, co-expression of OS-9 suppressed the degradation of NHK-QQQ, as in mock-transfected cells (Fig. 4H, lanes 7–9, quantified in the graph), probably due to the stabilization of transfected SEL1L. Indeed, transfected S-SEL1L, which disappeared with a half-life of ~45 min, was dramatically stabilized by co-expression of OS-9 (Fig. 4I, quantified in the graph).

Endogenous SEL1L is degraded under ER stress conditions

We next searched for conditions that enhance the degradation of endogenous SEL1L. SEL1L is

upregulated by ER stress [25]; therefore, we treated HEK293 cells with the pharmacological ER stress inducers thapsigargin (Ca^{2+}-ATPase inhibitor) and tunicamycin (protein glycosylation inhibitor). Upon inhibition of proteasome activity, SEL1L degradation intermediates were detected as observed in cells transfected with SEL1L (Fig. 5A, lanes 4 and 6). We also depleted endogenous HRD1 or both OS-9 and XTP3-B, which destabilized endogenous SEL1L. As expected, degradation intermediates of endogenous SEL1L were detected upon addition of MG132 (Fig. 5B, lanes 4 and 6). These results suggest that transfected SEL1L represents the dynamics of endogenous SEL1L.

We confirmed that co-transfected S-SEL1L and HRD1-myc formed a complex that was sensitive to the detergents used for cell lysis (Fig. 5C) [17], similar to the interaction of SEL1L-HA and HRD1-myc [14]. Both SEL1L-HA and S-SEL1L associated with HRD1-myc were targeted to the ER membrane, as verified by alkaline extraction of microsomal membranes (Fig. 5D, lane 3). Although transfected S-SEL1L was unstable and rapidly degraded, it was greatly stabilized by co-expression of HRD1-myc (Fig. 5E), as observed for SEL1L-HA and HRD1-myc [14]. We previously showed that ERAD of NHK-QQQ is inhibited by transient expression of HRD1-myc and is restored by co-expression of HRD1-myc and SEL1L-HA, indicating that the transfected SEL1L-HA–HRD1-myc complex is functional [14]. Similarly, co-expression of S-SEL1L and HRD1-myc recovered NHK degradation (Fig. 5F). Collectively, these results indicate

that transfected S-SEL1L and SEL1L-HA localize to the ER membrane and function by forming a complex with HRD1-myc.

The C-terminal Pro-rich region of SEL1L is required for generation of SEL1L degradation intermediates

Because SEL1L is involved in tumor progression [26], we next analyzed the expression of SEL1L protein in several human cancer cell lines: HeLa (cervical epithelial cancer), HepG2 (hepatocellular carcinoma), RD (rhabdomyosarcoma), and Capan2 (pancreas cancer). The levels of endogenous SEL1L varied among the cell lines and did not increase upon addition of proteasome inhibitor (Fig. 6A). However, transiently expressed SEL1L-HA generated degradation intermediates in all cell lines examined, as in HEK 293 cells (Fig. 6B). These results suggest that endogenous SEL1L is stabilized in those cancer cell lines, whereas rapid fragmentation of SEL1L occurs when SEL1L is transiently overexpressed.

SEL1L has a Pro-rich region at the C-terminus [26] (Suppl. Fig. 1) that also contains two Arg residues. We considered the possibility that this region interacts with the proteasome and interferes with its function, similar to the Pro- and Arg-rich peptide [27]. To analyze the effect of the Pro-rich region for generation of SEL1L degradation intermediates, we constructed plasmids lacking this region (SEL1LΔPR-HA). SEL1LΔPR-HA expressed in HEK 293 cells produced

degradation fragments in the presence of MG132 (Fig. 6C). Each fragment migrated faster than the corresponding band generated from SEL1L-HA (Fig. 6C, compare red and black angle brackets), indicating that cleavage occurred at the same positions in the SEL1L protein. However, the signal intensity of the degradation intermediates was dramatically reduced in SEL1LΔPR-HA, suggesting that the C-terminal Pro-rich region of SEL1L increases the protein's stability.

Degradation of the ERAD substrate NHK-QQQ was elevated when the half-life of SEL1L is reduced [14] (Fig. 4). Consistent with this, NHK-QQQ disappeared more rapidly in cells expressing SEL1LΔPR-HA than in those transfected with SEL1L-HA (Fig. 6D, left panel). SEL1LΔPR-HA was rapidly degraded, as measured by pulse-chase experiments (Fig. 6D, right panel). Collectively, these results suggest that the C-terminal Pro-rich region is responsible for the appearance of SEL1L degradation intermediates.

SEL1L degradation intermediates stimulate cytosolic polyQ aggregation

SEL1L has eleven SLRs [16] (Fig. 1A), which resemble tetratricopeptide repeats [28]. Given that SLR may be involved in protein–protein interactions, we reasoned that cytosolically accumulated SEL1L SLRs associate with misfolded cytosolic proteins. Polyglutamine (polyQ)-expanded proteins, pathogenic peptides of Huntington's disease and other neurodegenerative diseases [11, 12], form large aggregates in the cytosol or nucleus. When we analyzed the effect of SEL1L

degradation intermediates on polyQ aggregation, we used Htt-polyQ76-GFP, which consists of a polyQ76 stretch in Htt exon 1 fused to EGFP and the FLAG epitope; the fusion protein forms large aggregates in HEK 293 cells [29]. The number of cells that formed cytosolic inclusions of Htt-polyQ76-GFP increased upon addition of MG132 and was dramatically increased by co-transfection of SEL1L-HA in the presence of proteasome inhibitor (Fig. 7A, quantified in B). Expression of ΔssSEL1L-HA also stimulated polyQ aggregation (Fig. 7A, quantified in B), suggesting that degradation intermediates of SEL1L can associate with polyQ fibrils formed in the cytoplasm.

Transfected SEL1L-HA in HeLa cells was expressed in the ER, as confirmed by co-localization with the ER marker calreticulin (CRT) (Fig. 7C, upper left panels, MG132 -), but not with the cytosolic marker HSP/HSC70 (Fig. 7C, upper right panels, MG132 -). However, in the presence of MG132, anti-HA antibody revealed cytosolic staining that did not merge with that of CRT, in addition to ER localization (Fig. 7C, upper left panels, MG132 +). Co-localization of HA signals with HSP/HSC70 signals increased accordingly (Fig. 7C, upper right panels, MG132 +). These results are consistent with the subcellular localization of SEL1L-HA and its degradation intermediates, as determined by subcellular fractionation (Fig. 2). As expected, ΔssSEL1L-HA was stained in the cytosol when proteasome inhibitor was added (Fig. 7C, lower panels, MG132 +), although only a faint HA signal was detected in the absence of proteasome inhibitor (Fig. 7C,

lower panels, MG132 -). SEL1L-HA transfected in HEK 293 cells exhibited similar subcellular localization (data not shown). These results suggest that SEL1L degradation intermediates generated in the cytosol interacted with Htt-polyQ76-GFP and promoted aggregate formation.

SEL1L degradation intermediates associate with cytosolic polyQ aggregates

To explore the interaction of SEL1L degradation intermediates with polyQ aggregation, we next investigated whether SEL1L-HA was co-localized with Htt-polyQ76-GFP. In the absence of MG132, large cytosolic polyQ aggregates were detected outside the ER, which was stained by the anti-HA antibody (Fig. 8A, >80% in a total of 86 cells in two independent experiments). However, in the presence of MG132, polyQ inclusions were surrounded by the HA signal, suggesting that SEL1L-HA degradation intermediates accumulated on the surface of polyQ aggregates (>95%, in a total of 94 cells from two independent experiments) (Fig. 8B). In the absence of MG132, ~10% cells exhibited a ring-like pattern. The appearance of ring-like structures around polyQ aggregates was reminiscent of patterns observed for the cytosolic chaperone Hsp70 or transcription factors such as TATA-binding protein and CREB-binding protein [29, 30]. In cells expressing ΔssSEL1L-HA, in addition to the ring-like structure (~70%, in 118 cells from three independent experiments) (Fig. 8C, left panel), ~15% of the aggregate cores exhibited a nearly complete overlap in the localization of the two proteins (Fig. 8C, right

panel), reminiscent of the co-localization of expanded polyQ aggregates with Htt-polyQ23 [30] or the cytosolic chaperones DNAJB6 and DNAJB8 [31]. Similarly, in HeLa cells transfected with SEL1L-HA or ΔssSEL1L-HA, degradation intermediates exhibited both ring-like structures (>90% in a total of 62 SEL1L-HA-expressing cells from three independent experiments, and >50% in a total of 92 ΔssSEL1L-HA-expressing cells from three independent experiments) and co-localization in the core of polyQ aggregates (~20% in a total of 92 ΔssSEL1L-HA-expressing cells from two independent experiments), although the efficiency of inclusion formation was low in this cell line (Fig. 8D).

PolyQ-23-GFP, which contains a short polyQ stretch, usually does not form aggregates. However, in cells co-transfected with SEL1L-HA or ΔssSEL1L-HA, large cytosolic aggregates were detected in the presence of MG132 (Fig. 8E, F). The aggregates had a unique sponge-like shape distinct from the typical morphology of polyQ76-GFP. HA signal was co-localized or accumulated around the Htt-polyQ23-GFP core. These results indicate that SEL1L degradation fragments binds to aggregation-prone proteins like Htt-polyQ-76-GFP in the cytosol and induce co-fibrillization with otherwise soluble Htt-polyQ23-GFP.

The SEL1L SLR promotes cytosolic polyQ aggregation

Finally, we asked whether the characteristic Sel1-like repeat (SLR) of SEL1L is critical for polyQ

aggregation. To this end, we expressed a SEL1L fragment containing only SLR 5–9 (SEL1L-R5-9-HA) in the cytosol, as this region was successfully crystallized [32]. Co-expression of SEL1L-R5-9-HA promoted polyQ aggregation in the presence of proteasome inhibitor (Fig. 9A, quantified in B), and HA signals were observed surrounding the Htt-polyQ76-GFP aggregates (Fig. 9C).

We then confirmed polyQ aggregate formation by filter-trap assay. In cells co-transfected with SEL1L-HA, Htt-polyQ76-GFP aggregation was promoted by the addition of proteasome inhibitor, whereas no aggregates were detected in cells expressing Htt-polyQ23-GFP (Fig. 9D). Similarly, in cells co-expressing ΔssSEL1L-HA or SEL1L-R5-9-HA, Htt-polyQ76-GFP aggregation was more prominent than in mock-transfected cells in the presence of MG132 (Fig. 9E). Collectively, these results suggest that the SEL1L SLR, which must be released into the cytosol after retrotranslocation from the ER, interacts with Htt-polyQ76-GFP and augments cytosolic inclusions.

Discussion

A large membrane assembly centered on the HRD1–SEL1L ubiquitin ligase complex in the ER membrane regulates the mammalian ERAD. SEL1L is inherently unstable and is degraded by ERAD unless it forms a complex with HRD1 (Fig. 9F) [14, 15]. Transiently expressed SEL1L generates multiple degradation intermediates when proteasome activity is inhibited. In this study, we analyzed the SEL1L disposal process in detail. We found similar degradation intermediates of endogenous SEL1L in cells exposed to ER stress or treated with siRNA targeting its associating proteins (Fig. 5A, B). We concluded that SEL1L that failed to bind the ER-luminal lectins OS-9 and XTP3-B or HRD1 is retrotranslocated into the cytoplasm, where it is rapidly digested by the proteasome to prevent augmentation of toxic aggregates. Our results also suggest that the association of SEL1l with HRD1 may be more dynamically regulated, enabling the SEL1L-lectin complex, which only contains the single transmembrane region in SEL1L, to move more freely than the SEL1L–HRD1 complex in order to surveil the ER lumen for misfolded proteins (Fig. 9F). Endogenous SEL1L was destabilized by knockdown of OS-9 and XTP3-B (Fig. 4D–G), further supporting the dynamic regulation of SEL1L. Although overexpression of either OS-9 or XTP3-B stabilized transiently transfected SEL1L, depletion of XTP3-B did not suppress the expression of endogenous SEL1L, whereas knockdown of OS-9 alone or both OS-9 and XTP3-

B decreased the level of endogenous SEL1L (Fig. 4). Destabilization of SEL1L by double-knockout of OS-9 and XTP3-B was also reported by van der Goot et al. [33] during the preparation of this manuscript. In that report, however, SEL1L was not destabilized in OS-9 KO cells [33]. This discrepancy may be explained by differences in study design: in our study we used a transient knockdown, whereas van der Goot *et al.* established a stable KO cell line in which some kind of compensation mechanism may have been activated.

Using either N-terminally S-tagged or C-terminally HA-tagged SEL1L, we detected both N-terminal and C-terminal fragments during the degradation process. The pattern of the fragments was similar under all conditions tested, suggesting that SEL1L is cleaved at defined positions. Because the level of degradation intermediates did not increase during the chase period of a pulse-chase analysis (Fig. 1E, and [15]), we speculate that SEL1L is not cleaved by cytosolic proteases, but rather truncated by the function of proteasome. Given that SEL1L lacking the C-terminal Pro-rich region was degraded more rapidly, this region might interact with the proteasome and partly inhibit proteasome function, in a manner similar to Pro- and Arg-rich peptides that inhibit the proteasome [27]. Upon inhibition of proteasomal activity, most ERAD substrates accumulate in the ER, but deglycosylated intermediates of MHC class I molecules are detected [21]. SEL1L degradation intermediates contained fragments of various molecular weights, and the longest fragment migrated at the same position as deglycosylated SEL1L, as confirmed by PNGaseF

treatment (data not shown), as well as by treatment with the cytosolic PNGase inhibitor Z-VAD-FMK (Fig. 3C).

We also found that co-expression of SEL1L stimulated cytosolic Htt-polyQ aggregation when proteasome function was inhibited. Cytosolically expressed SEL1L (ΔssSEL1L-HA) or a plasmid expressing only SEL1L SLR 5–9 (Fig. 1A) also promoted aggregation formation. Because SLR 5–9 has been successfully crystalized [32], we expect that cytosolically expressed SLR 5–9 would maintain its domain structures, allowing interactions with other proteins [16]. Similarly, the TPR domain of CHIP is required for the aggregation of polyQ-expanded ataxin-1 [34]. Immunostaining revealed that SEL1L degradation intermediates, as well as SLR 5–9, formed a ring-like structure surrounding the Htt-polyQ aggregates. In addition, we detected co-staining of Htt-polyQ76-GFP and SEL1L fragments in the entire aggregates in cells co-transfected with ΔssSEL1L-HA. In cells expressing Htt-polyQ23, similar co-staining throughout entire aggregates was frequently observed. Thus, SEL1L degradation intermediates interact with aggregation-prone proteins probably through the SLR domain. Although endogenous SEL1L expressed in HEK 293 cells and several cancer cell lines were stable (Fig. 6A), endogenous SEL1L in U937 cells was unstable and rapidly degraded by the proteasome [35]. Recently, massive degradation of the yeast homolog Hrd3 was reported by the self-remodeling of the HRD complex [36]. Here, we found that endogenous SEL1L is degraded under ER stress conditions

such as those induced by thapsigargin or tunicamycin treatment. Expression of SEL1L is upregulated by the UPR [25]; therefore, SEL1L protein is likely to be degraded under certain pathophysiological conditions. PolyQ-expanded Htt impairs ERAD and induces ER stress [13]; conversely, ER stress triggers cytosolic aggregation of intrinsically aggregation-prone proteins [37]. Thus, protein homeostasis across subcellular compartments is tightly regulated. Collectively, our results demonstrate that degradation fragments of ER proteins released during ERAD can promote massive aggregation of unstable proteins in the cytosol.

Methods

Cell culture, transfection, and drug treatment

HEK293, HeLa, HepG2, RD, and Capan2 cells were cultured in DMEM supplemented with 10% fetal bovine serum and antibiotics, as described previously [14]. Plasmids were purified using the Maxi-prep Plasmid Purification kit (Qiagen, Valencia, CA, USA) and transfected into cells using Lipofectamine 2000 (Invitrogen, Waltham, MA, USA), ViaFect (Promega, Madison, WI, USA), or polyethyleneimine (branched; Sigma-Aldrich, St Louis, MO, USA).

MG-132 (Peptide Institute, Osaka, Japan), Z-VAD-FMK (Peptide Institute), MNS-873 (Cayman Chemical Company, Ann Arbor, MI, USA), thapsigargin (Sigma-Aldrich), and tunicamycin (Sigma-Aldrich) were dissolved in DMSO and added to the medium at final concentrations of 20 μM, 30 μM, 2.5 μM, 1.5 μM, and 5 μg/ml, respectively. Cells were incubated with each drug for 6 h, unless described otherwise in the legends. Cycloheximide (Nacalai Tesque, Kyoto, Japan) was dissolved in phosphate-buffered saline (PBS), and added to the medium at a final concentration of 100 μM.

Construction of plasmids

S-SEL1L was kindly provided by Dr. R. Kopito (Stanford University, USA) [17]. Htt-polyQ76-GFP and Htt-polyQ23-GFP were generous gift from Dr. A. Kitamura (Hokkaido University, Japan) [38]. ΔssSEL1L-HA was constructed by amplifying human SEL1L lacking the N-terminal signal sequence (amino acids 2–21), followed by subcloning into the *Hin*dIII–*Eco*RI site of vector pMH (Roche Applied Science, Mannheim, Germany). SEL1LΔPR-HA was generated by amplifying human SEL1L lacking the C-terminal Pro-rich region (amino acids 770–793) and subcloning into the *Hin*dIII–*Eco*RI site of pMH. To construct SEL1L-R5-9-HA, synthesized DNA containing SLR 5–9 (amino acids 352–537, gBlock; IDT, Coralville, IA, USA) was cloned into the *Eco*RI site of pMH.

Details of the NHK-QQQ, SEL1L-HA, FolA-S-HA, OS-9v2-HA, and XTP3B-HA were constructed as described previously [14, 39-41].

siRNA oligos

The Stealth siRNA oligo (Invitrogen) sequences used were as follows: OS-9 #2, 5'-GGAAACGCUGCUGUCCAGUUUGUUA-3'; OS-9 #3, 5'-GGAGGAGGAAACACCUGCUUACCAA-3' [40]; XTP3-B #2, 5'-UUUCCCACUAUCCUUGUCCUCAUGG-3'; XTP3-B #3, 5'-UUUCCAUGACAUACUUCGUAAGUCC-3' [41]; and HRD1 5'-

UUGAUCUGCAGCAUGGCGGCGUCCA-3'. Medium-GC negative control siRNA (Invitrogen) was used as a negative control.

Antibodies

Mouse monoclonal anti-HRD1/synoviolin antibody was kindly provided by Dr. T. Nakajima (St. Marianna University School of Medicine, Japan), and rabbit anti-HSP70/HSC70 antibody was a generous gift from Dr. K. Ohtsuka (Chubu University, Japan). Rabbit anti-SEL1L antibody was generated as described previously [15]. Rabbit anti-GFP antibody was described elsewhere [42]. Other antibodies were purchased from the following suppliers: rabbit polyclonal anti-HA (Recenttec, Tokyo, Japan), rabbit polyclonal anti-c-myc (Santa Cruz Biotechnology, Dallas, TX, USA), mouse monoclonal anti-c-myc (9E10, Santa Cruz Biotechnology), mouse monoclonal anti-HA (HA-7) (Sigma-Aldrich), rabbit anti–S-tag (Abcam, Cambridge, UK), mouse anti-FLAG (M2) (Sigma-Aldrich), rabbit monoclonal anti–OS-9 (Abcam), rabbit anti–XTP3-B (Sigma-Aldrich), rabbit anti-HRD1/synoviolin (Proteintech, Rosemont, IL, USA), rabbit anti-α_1AT (DAKO, Glostrup, Denmark), mouse anti-actin (Millipore, Billerica, MA, USA), rabbit anti-calnexin (Enzo Life Sciences, Farmingdale, NY, USA), rabbit anti-PDI (Enzo Life Sciences), mouse anti-BiP (BD Transduction Laboratories), peroxidase-conjugated sheep anti-α_1AT (The Binding Site, Birmingham, UK), horseradish peroxidase-conjugated anti-rabbit IgG (BTI,

Thermo Fisher), and horseradish peroxidase-conjugated anti-mouse IgG (Zymed Laboratories Inc., Thermo Fisher). Clean-Blot IP Detection Reagent was purchased from Thermo Fisher Scientific (Rockford, IL, USA).

Subcellular protein fractionation

HEK 293 cells were fractionated using the Subcellular Fractionation Kit for Cultured Cells (Thermo Fisher Scientific). Alternatively, HEK 293 cells were homogenized in an isotonic buffer (250 mM sucrose, 10 mM HEPES (pH 7.4), and 1 mM $CaCl_2$) by passing them through a 30-G needle as described previously [43]. Briefly, homogenates were centrifuged at 300 × g for 5 min, and the supernatant was re-centrifuged at 1,500 × g for 5 min. The cytosol and microsomes were fractionated by ultracentrifugation of the supernatant at 100,000 × g for 1 h in a Beckman TL100.1 rotor. Proteins were separated by SDS-PAGE and analyzed by Western blotting.

Metabolic labeling and immunoprecipitation

Metabolic labeling of HEK293 cells, pulse-chase experiments, and immunoprecipitation were performed as described previously [14]. Radioisotope incorporation was visualized on a Typhoon FLA PhosphorImager (GE Healthcare Bio-Sciences, Uppsala, Sweden), and the signal intensity of each protein was quantified using the ImageQuant software (GE Healthcare Bio-Sciences).

Western blotting

Cells were lysed in a buffer containing 1% NP-40 and protease inhibitors (0.2 mM 4-(2-aminoethyl)benzenesulfonyl fluoride, 2 mM N-ethylmaleimide, 1 μg/ml leupeptin, and 1 μg/ml pepstatin) unless described otherwise in the legends. Cell extracts dissolved in 1 × Laemmli's buffer containing 0.1 M DTT were separated by 10% SDS-PAGE and were blotted onto PVDF membranes (Millipore). For electrophoresis under non-reducing conditions, cell extracts alkylated by NEM were dissolved in 1 × Laemmli's buffer lacking DTT. After blocking with Blocking-One solution (Nacalai Tesque), the membranes were incubated with antibodies diluted in Can Get Signal solution (Toyobo) or PBS containing 0.1% Tween-20 and 5% Blocking-One solution. Specific signals were detected using Pierce Western Blotting Substrate (Thermo Fisher Scientific) and visualized on a LAS-4000 (GE Healthcare Bio-Sciences). Signal intensity was quantified using the ImageQuant software.

Live-cell imaging

Cells were grown on 35 mm plastic dishes (Falcon) and transfected with plasmids. Images were acquired using LAS AF (Leica Microsystems, Wetzlar, Germany) using PL FLUOROTARL 40x (NA 0.60) objective lens. The temperature was maintained at 37°C with 5% CO_2 using a

microscope incubator (TOKAI HIT CO., LTD, Shizuoka, Japan). Nuclei were stained with Hoechst 33342 (Dojindo, Japan) for 30 min prior to microscopic observation.

Immunocytochemistry

HEK 293 and HeLa cells were plated on a coverslip, and the indicated plasmids were transfected. Cells were fixed with 4% paraformaldehyde for 15 min at room temperature, permeabilized with 0.2% Triton X-100 for 4 min on ice, and then stained with mouse monoclonal anti-HA (HA-7) and rabbit polyclonal anti-calreticulin (Affinity Bioreagents, Golden, CO, USA) or anti-HSP/HSC70 as the primary antibodies. In cells expressing Htt-polyQ-GFP and SEL1L-HA, ΔssSEL1L-HA, or SEL1L-R5-9-HA, mouse monoclonal anti-HA (HA-7) and rabbit polyclonal anti-GFP antibodies were used. Alexa Fluor 488-conjugated anti-rabbit and Alexa Fluor 594-conjugated anti-mouse were used as secondary antibodies (Clontech, Takara Bio). Nuclei were counterstained with DAPI. Fluorescence images were captured through a HC PL APO 63x (NA 1.4) objective lens at 1024 × 1024 dpi on a TCS SP8 microscope (Leica Microsystems).

Filter-trap assay

Filter-trap assays were performed as described previously [38, 44]. Briefly, HEK 293 cells were collected in a buffer containing 0.5% Triton X-100, sonicated, and lysed in a buffer containing

1% SDS. Cell lysates were serially diluted and applied to a cellulose acetate membrane (pore size, 0.2 μM). SDS-resistant polyQ aggregation was detected using anti-GFP antibody.

Author contributions

NH and IW planned the experiments; TH, KH, and NH performed the experiments; NH and IW analyzed the data and wrote the manuscript.

Acknowledgments

This work was supported by a grant-in-aid for Scientific Research (KAKENHI) from the Ministry of Education, Culture, Sports, Science, and Technology of Japan (26440096 to N.H. and 17K07311 to I.W.). We thank Azusa Ujiie for counting of the polyQ aggregates. We also thank Dr. F. Tokunaga and Dr. D. Oikawa (Osaka City University), Dr. K. Iwai (Kyoto University), Dr. A. Kitamura (Hokkaido University), and Dr. K. Nagai (Osaka University) for useful discussions and suggestions about experiments.

Conflicts of interest

The authors have no conflicts of interest to declare.

References

1. Hipp, M. S., Kasturi, P. & Hartl, F. U. (2019) The proteostasis network and its decline in ageing, *Nat Rev Mol Cell Biol.* **20**, 421-435.
2. Ellgaard, L., McCaul, N., Chatsisvili, A. & Braakman, I. (2016) Co- and Post-Translational Protein Folding in the ER, *Traffic.* **17**, 615-38.
3. Preston, G. M. & Brodsky, J. L. (2017) The evolving role of ubiquitin modification in endoplasmic reticulum-associated degradation, *Biochem J.* **474**, 445-469.
4. Berner, N., Reutter, K. R. & Wolf, D. H. (2018) Protein Quality Control of the Endoplasmic Reticulum and Ubiquitin-Proteasome-Triggered Degradation of Aberrant Proteins: Yeast Pioneers the Path, *Annu Rev Biochem*.
5. Carvalho, P., Goder, V. & Rapoport, T. A. (2006) Distinct ubiquitin-ligase complexes define convergent pathways for the degradation of ER proteins, *Cell.* **126**, 361-73.
6. Wu, X., Siggel, M., Ovchinnikov, S., Mi, W., Svetlov, V., Nudler, E., Liao, M., Hummer, G. & Rapoport, T. A. (2020) Structural basis of ER-associated protein degradation mediated by the Hrd1 ubiquitin ligase complex, *Science.* **368**.
7. Ruggiano, A., Foresti, O. & Carvalho, P. (2014) Quality control: ER-associated degradation: protein quality control and beyond, *J Cell Biol.* **204**, 869-79.
8. Hipp, M. S., Park, S. H. & Hartl, F. U. (2014) Proteostasis impairment in protein-misfolding and -aggregation diseases, *Trends Cell Biol.* **24**, 506-14.
9. Chiti, F. & Dobson, C. M. (2017) Protein Misfolding, Amyloid Formation, and Human Disease: A Summary of Progress Over the Last Decade, *Annu Rev Biochem.* **86**, 27-68.
10. Labbadia, J. & Morimoto, R. I. (2015) The biology of proteostasis in aging and disease, *Annu Rev Biochem.* **84**, 435-64.
11. Lieberman, A. P., Shakkottai, V. G. & Albin, R. L. (2019) Polyglutamine Repeats in Neurodegenerative Diseases, *Annu Rev Pathol.* **14**, 1-27.
12. Orr, H. T. & Zoghbi, H. Y. (2007) Trinucleotide repeat disorders, *Annu Rev Neurosci.* **30**, 575-621.
13. Duennwald, M. L. & Lindquist, S. (2008) Impaired ERAD and ER stress are early and specific events in polyglutamine toxicity, *Genes Dev.* **22**, 3308-19.
14. Hosokawa, N. & Wada, I. (2016) Association of the SEL1L protein transmembrane domain with HRD1 ubiquitin ligase regulates ERAD-L, *Febs j.* **283**, 157-72.
15. Iida, Y., Fujimori, T., Okawa, K., Nagata, K., Wada, I. & Hosokawa, N. (2011) SEL1L protein critically determines the stability of the HRD1-SEL1L endoplasmic reticulum-associated

degradation (ERAD) complex to optimize the degradation kinetics of ERAD substrates, *J Biol Chem.* **286**, 16929-39.

16. Mittl, P. R. & Schneider-Brachert, W. (2007) Sel1-like repeat proteins in signal transduction, *Cell Signal.* **19**, 20-31.

17. Christianson, J. C., Shaler, T. A., Tyler, R. E. & Kopito, R. R. (2008) OS-9 and GRP94 deliver mutant alpha1-antitrypsin to the Hrd1-SEL1L ubiquitin ligase complex for ERAD, *Nat Cell Biol.* **10**, 272-82.

18. Kang, S. W., Rane, N. S., Kim, S. J., Garrison, J. L., Taunton, J. & Hegde, R. S. (2006) Substrate-specific translocational attenuation during ER stress defines a pre-emptive quality control pathway, *Cell.* **127**, 999-1013.

19. Misaghi, S., Pacold, M. E., Blom, D., Ploegh, H. L. & Korbel, G. A. (2004) Using a small molecule inhibitor of peptide: N-glycanase to probe its role in glycoprotein turnover, *Chem Biol.* **11**, 1677-87.

20. Suzuki, T. (2007) Cytoplasmic peptide:N-glycanase and catabolic pathway for free N-glycans in the cytosol, *Semin Cell Dev Biol.* **18**, 762-9.

21. Wiertz, E. J., Jones, T. R., Sun, L., Bogyo, M., Geuze, H. J. & Ploegh, H. L. (1996) The human cytomegalovirus US11 gene product dislocates MHC class I heavy chains from the endoplasmic reticulum to the cytosol, *Cell.* **84**, 769-79.

22. Wolf, D. H. & Stolz, A. (2012) The Cdc48 machine in endoplasmic reticulum associated protein degradation, *Biochim Biophys Acta.* **1823**, 117-24.

23. Magnaghi, P., D'Alessio, R., Valsasina, B., Avanzi, N., Rizzi, S., Asa, D., Gasparri, F., Cozzi, L., Cucchi, U., Orrenius, C., Polucci, P., Ballinari, D., Perrera, C., Leone, A., Cervi, G., Casale, E., Xiao, Y., Wong, C., Anderson, D. J., Galvani, A., Donati, D., O'Brien, T., Jackson, P. K. & Isacchi, A. (2013) Covalent and allosteric inhibitors of the ATPase VCP/p97 induce cancer cell death, *Nat Chem Biol.* **9**, 548-56.

24. Xu, C. & Ng, D. T. (2015) Glycosylation-directed quality control of protein folding, *Nat Rev Mol Cell Biol.* **16**, 742-52.

25. Cattaneo, M., Baronchelli, S., Schiffer, D., Mellai, M., Caldera, V., Saccani, G. J., Dalpra, L., Daga, A., Orlandi, R., DeBlasio, P. & Biunno, I. (2014) Down-modulation of SEL1L, an unfolded protein response and endoplasmic reticulum-associated degradation protein, sensitizes glioma stem cells to the cytotoxic effect of valproic acid, *J Biol Chem.* **289**, 2826-38.

26. Biunno, I., Cattaneo, M., Orlandi, R., Canton, C., Biagiotti, L., Ferrero, S., Barberis, M., Pupa, S. M., Scarpa, A. & Menard, S. (2006) SEL1L a multifaceted protein playing a role in tumor progression, *J Cell Physiol.* **208**, 23-38.

27. Anbanandam, A., Albarado, D. C., Tirziu, D. C., Simons, M. & Veeraraghavan, S. (2008) Molecular basis for proline- and arginine-rich peptide inhibition of proteasome, *J Mol Biol.* **384**,

219-27.
28. Sikorski, R. S., Boguski, M. S., Goebl, M. & Hieter, P. (1990) A repeating amino acid motif in CDC23 defines a family of proteins and a new relationship among genes required for mitosis and RNA synthesis, *Cell.* **60**, 307-17.
29. Kim, S., Nollen, E. A., Kitagawa, K., Bindokas, V. P. & Morimoto, R. I. (2002) Polyglutamine protein aggregates are dynamic, *Nat Cell Biol.* **4**, 826-31.
30. Matsumoto, G., Kim, S. & Morimoto, R. I. (2006) Huntingtin and mutant SOD1 form aggregate structures with distinct molecular properties in human cells, *J Biol Chem.* **281**, 4477-85.
31. Gillis, J., Schipper-Krom, S., Juenemann, K., Gruber, A., Coolen, S., van den Nieuwendijk, R., van Veen, H., Overkleeft, H., Goedhart, J., Kampinga, H. H. & Reits, E. A. (2013) The DNAJB6 and DNAJB8 protein chaperones prevent intracellular aggregation of polyglutamine peptides, *J Biol Chem.* **288**, 17225-37.
32. Jeong, H., Sim, H. J., Song, E. K., Lee, H., Ha, S. C., Jun, Y., Park, T. J. & Lee, C. (2016) Crystal structure of SEL1L: Insight into the roles of SLR motifs in ERAD pathway, *Sci Rep.* **6**, 20261.
33. van der Goot, A. T., Pearce, M. M. P., Leto, D. E., Shaler, T. A. & Kopito, R. R. (2018) Redundant and Antagonistic Roles of XTP3B and OS9 in Decoding Glycan and Non-glycan Degrons in ER-Associated Degradation, *Mol Cell.* **70**, 516-530 e6.
34. Choi, J. Y., Ryu, J. H., Kim, H. S., Park, S. G., Bae, K. H., Kang, S., Myung, P. K., Cho, S., Park, B. C. & Lee, D. H. (2007) Co-chaperone CHIP promotes aggregation of ataxin-1, *Mol Cell Neurosci.* **34**, 69-79.
35. Mueller, B., Lilley, B. N. & Ploegh, H. L. (2006) SEL1L, the homologue of yeast Hrd3p, is involved in protein dislocation from the mammalian ER, *J Cell Biol.* **175**, 261-70.
36. Neal, S., Syau, D., Nejatfard, A., Nadeau, S. & Hampton, R. Y. (2020) HRD Complex Self-Remodeling Enables a Novel Route of Membrane Protein Retrotranslocation, *iScience.* **23**, 101493.
37. Hamdan, N., Kritsiligkou, P. & Grant, C. M. (2017) ER stress causes widespread protein aggregation and prion formation, *J Cell Biol.* **216**, 2295-2304.
38. Kitamura, A., Kubota, H., Pack, C. G., Matsumoto, G., Hirayama, S., Takahashi, Y., Kimura, H., Kinjo, M., Morimoto, R. I. & Nagata, K. (2006) Cytosolic chaperonin prevents polyglutamine toxicity with altering the aggregation state, *Nat Cell Biol.* **8**, 1163-70.
39. Hirao, K., Natsuka, Y., Tamura, T., Wada, I., Morito, D., Natsuka, S., Romero, P., Sleno, B., Tremblay, L. O., Herscovics, A., Nagata, K. & Hosokawa, N. (2006) EDEM3, a soluble EDEM homolog, enhances glycoprotein endoplasmic reticulum-associated degradation and mannose trimming, *J Biol Chem.* **281**, 9650-8.

40. Hosokawa, N., Kamiya, Y., Kamiya, D., Kato, K. & Nagata, K. (2009) Human OS-9, a lectin required for glycoprotein endoplasmic reticulum-associated degradation, recognizes mannose-trimmed N-glycans, *J Biol Chem.* **284**, 17061-8.

41. Hosokawa, N., Wada, I., Nagasawa, K., Moriyama, T., Okawa, K. & Nagata, K. (2008) Human XTP3-B Forms an Endoplasmic Reticulum Quality Control Scaffold with the HRD1-SEL1L Ubiquitin Ligase Complex and BiP, *J Biol Chem.* **283**, 20914-24.

42. Sakurai, C., Itakura, M., Kinoshita, D., Arai, S., Hashimoto, H., Wada, I. & Hatsuzawa, K. (2018) Phosphorylation of SNAP-23 at Ser95 causes a structural alteration and negatively regulates Fc receptor-mediated phagosome formation and maturation in macrophages, *Mol Biol Cell.* **29**, 1753-1762.

43. Wada, I., Kai, M., Imai, S., Sakane, F. & Kanoh, H. (1997) Promotion of transferrin folding by cyclic interactions with calnexin and calreticulin, *EMBO J.* **16**, 5420-32.

44. Wanker, E. E., Scherzinger, E., Heiser, V., Sittler, A., Eickhoff, H. & Lehrach, H. (1999) Membrane filter assay for detection of amyloid-like polyglutamine-containing protein aggregates, *Methods Enzymol.* **309**, 375-86.

Figure legends

Figure 1. SEL1L degradation intermediates can be detected in cells treated with proteasome inhibitor.

(A) Schematic representation of the domain organization of SEL1L protein. FN type II, fibronectin type II domain; TM, transmembrane.

(B) HEK 293 cells were transfected with wild-type SEL1L, S-SEL1L, or SEL1L-HA, and then treated with MG132 for 6 h. Cells were extracted in a buffer containing 1% NP-40, and supernatant was collected. After separation by 10% SDS-PAGE, specific signals were detected by Western blotting. Blue, black, and gray arrows indicate endogenous SEL1L, full-length S-SEL1L, and full-length SEL1L-HA, respectively. Angle brackets denote the SEL1L degradation intermediates. Asterisks show signals non-specifically detected by the antibodies. Lane numbers in parentheses indicate the same sample loaded in the left panel.

(C) Same as in A, except that cells were transfected with FolA-S-HA, which was detected with anti-HA-tag antibody. Arrow indicates full-length FolA-S-HA.

(D) HEK 293 cells were transfected with WT SEL1L and HA-Ubiquitin, and SEL1L protein was immunoprecipitated with anti-SEL1L antibody. The bracket indicates ubiquitinated SEL1L protein detected by the anti-HA antibody. ** indicates rabbit IgG contained in the anti-sera used

for immunoprecipitation.

(E) Pulse-chase analysis of S-SEL1L expressed in HEK 293 cells. Cells were treated with MG132 for 3 h prior to metabolic labeling for 15 min (MG132 +) and chased for the indicated periods. Cell lysates were immunoprecipitated using anti–S-tag or anti-SEL1L antibodies. The arrow indicates full-length S-SEL1L, and the blue arrow indicates endogenous SEL1L. Angle brackets denote degradation intermediates of S-SEL1L. Asterisk indicates a non-specific signal in MG132-treated cells. Full-length S-SEL1L was quantified, and results are shown as means ± SD from three independent experiments. **, $P < 0.01$; ***, $P < 0.001$ (two-tailed Student's *t*-test, compared with cells without MG132 treatment).

Figure 2. SEL1L degradation intermediates accumulate in the cytosol.

(A–C) HEK 293 cells expressing SEL1L-HA or S-SEL1L were fractionated into cytosol (CE), membrane (ME), and nuclear extracts (NE), and separated by 10% SDS-PAGE. Specific signals were detected by Western blot using anti-SEL1L (A) or anti–S-tag antibodies (B), or antibodies against ER (calnexin [CNX]), and cytosolic proteins (actin, HSC70/HSP70) (C). Blue brackets and arrows indicate endogenous SEL1L and full-length S-SEL1L, respectively. Angle brackets denote SEL1L degradation intermediates. Lane numbers in parenthesis in (B) indicate the same samples loaded in (A) and (C).

(D, E) HEK 293 cells were homogenized by passing them through a 30-G needle in an isotonic buffer containing 250 mM sucrose, and then cytosol (S: supernatant) and microsome (P: pellet) fractions were separated by ultracentrifugation at 100,000 × g for 1 h. Specific signals were detected by Western blotting using anti-SEL1L (D) or anti–S-tag antibodies (E). Blue brackets, arrows and angle brackets are the same as in (A). Lane numbers in parenthesis in (E) indicate the same samples loaded in (D).

Figure 3. SEL1L degradation intermediates are reduced and deglycosylated.

(A) Extracts of HEK 293 cells expressing the indicated plasmids were separated by 10% SDS-PAGE under reducing (DTT +) or non-reducing (DTT -) conditions, and specific signals were detected by Western blot analysis using anti-SEL1L antibody. Blue, gray, and black arrows indicate endogenous SEL1L, full-length SEL1L-HA, and full-length S-SEL1L, respectively. Angle brackets denote SEL1L degradation intermediates.

(B) Western blot analysis of SEL1L-HA and ΔssSEL1L-HA expressed in HEK 293 cells. Arrow and arrowhead indicate full-length SEL1L-HA and ΔssSEL1L-HA, respectively. Angle brackets denote SEL1L degradation intermediates. Asterisks indicate non-specific signals detected by anti-HA antibody.

(C) HEK 293 cells expressing SEL1L-HA were treated with the PNGase inhibitor Z-VAD-FMK,

and cell lysates were analyzed by Western blot. Red angle brackets indicate SEL1L-HA degradation intermediates, whose migration was delayed by Z-VAD-FMK treatment.

(D) Two-dimensional isoelectric focusing (IEF) electrophoresis of SEL1L and ΔssSEL1L-HA. Cells extracted in a buffer containing 9.5 M urea were separated by IEF containing Ampholine (pH 3–10 and 4–7) in a tube gel, and then by 10% SDS-PAGE. After blotting onto PVDF membranes, specific signals were detected by Western blotting using anti-HA antibody (left panel). Double-headed arrows indicate full-length SEL1L-HA. Signals exhibiting different mobility in IEF are indicated by arrows (red in SEL1L-HA and black in ΔssSEL1L-HA). The same membranes were blotted sequentially with anti-actin (1), anti-BiP (2), and anti-calnexin (3, 3') antibodies to confirm comparable IEF separation on both membranes (right panel). Asterisks indicate non-specific signals detected by the antibodies.

(E) Same as in E, except that p97/VCP inhibitor MNS-873 was used.

Figure 4. Accumulation of SEL1L degradation intermediates is inhibited by co-expression of OS-9 and XTP3-B

(A–C) HEK 293 cells co-transfected with S-SEL1L and NHK-QQQ, OS-9v2-HA, or XTP3-B-HA were treated with proteasome inhibitor (MG132 +). Cell lysates were separated by 10% SDS-PAGE, and specific signals were detected by Western blotting with anti-SEL1L (A, upper panel),

anti-S-tag (A, lower panel), or indicated antibodies (B). Blue and black arrows indicate endogenous SEL1L and full-length S-SEL1L, respectively. Angle brackets denote SEL1L degradation intermediates.

(C) HEK 293 cells were co-transfected with WT SEL1L and the indicated ER proteins, and cell lysates were subjected to Western blotting with the indicated specific antibodies. MG132 was added from 6 h prior to harvest. Bracket indicates endogenous SEL1L and transfected full-length SEL1L, and angle brackets indicate SEL1L degradation intermediates.

(D–G) Western blot analysis of HEK 293 cells transfected with the indicated siRNAs for 48 h (D). Levels of endogenous SEL1L (E), OS-9 (F, including both OS-9v1 and v2), and XTP3-B (G) in D were quantified relative to cells treated with negative control siRNA (left-most lane). Results are shown as means ± SD from three independent experiments. ns, $P > 0.05$; **, $P < 0.01$; ***, $P < 0.001$ (two-tailed Student's *t*-test, compared with cells transfected with negative control siRNA).

(H) Pulse-chase analysis of NHK-QQQ degradation. HEK 293 cells co-transfected with NHK-QQQ, SEL1L, and OS-9v2-HA were metabolically labeled for 15 min and chased for the indicated period. NHK-QQQ was immunoprecipitated and separated by 10% SDS-PAGE. Radioisotope incorporation into NHK-QQQ is quantified in the graph. Error bars indicate means ± SD from three independent experiments. *, $P < 0.05$; ***, $P < 0.001$ (two-tailed Student's *t*-test, compared with cells co-transfected with SEL1L).

(I) Pulse-chase analysis of S-SEL1L degradation. Same as in A, except cells were transfected with S-SEL1L and OS-9v2-HA and immunoprecipitated using anti–S-tag or anti-HA antibodies. Radioactive incorporation to S-SEL1L was quantified in the graph. Error bars indicate means ± SD from three independent experiments. *, $P < 0.05$; **, $P < 0.01$ (two-tailed Student's *t*-test).

Figure 5. Degradation intermediates of endogenous SEL1L are detected in HEK 293 cells exposed to ER stress

(A) Western blot analysis of endogenous SEL1L upon treatement with thapsigargin (Tg) or tunicamycin (Tm). For clarity, the obtained images are shown in grayscale (top) or using the "fire" lookup table of ImageJ. Blue brackets indicate full-length endogenous SEL1L. Angle brackets denote SEL1L degradation intermediates. Double angle brackets indicate deglycosylated SEL1L.

(B) Western blot analysis of endogenous SEL1L in HEK 293 cells transfected with indicated siRNAs. Thirty hours after transfection of siRNAs, cells were treated with MG132 for 6 h (MG132 +). The same image is shown using the "fire" lookup table of ImageJ. The asterisk indicates a non-specific signal detected by anti–OS-9 antibody.

(C) Immunoprecipitation analysis of S-SEL1L and HRD1-myc co-expressed in HEK 293 cells. Cells were lysed in a buffer containing 1% NP-40 (NP-40) or 3% digitonin (Dig), and immunoprecipitated using anti-S-tag or anti-c-myc antibodies. ** indicates mouse IgG used for

immunoprecipitation.

(D) Alkaline extraction of SEL1L-HA, S-SEL1L and HRD1-myc expressed in HEK 293 cells. The microsomal fraction was prepared as in Fig. 2C and D from cells co-expressing SEL1L-HA and HRD1-myc (left panel) or S-SEL1L and HRD1-myc (right panel). After incubation in an alkaline solution containing 0.1 M Na_2CO_3 or in a buffer containing 1% NP-40, a supernatant (Sup) and pellet (Ppt) were fractionated by ultracentrifugation at 100,000 × g.

(E) Pulse-chase analysis of S-SEL1L co-expressed with or without HRD1-myc in HEK 293 cells. Cells were pulse-labeled for 15 min and chased for the indicated periods. Cell lysates were immunoprecipitated using anti–S-tag or anti-SEL1L antibodies. The bracket indicates full-length S-SEL1L. The blue arrow indicates endogenous SEL1L. Full-length S-SEL1L was quantified. Results are shown as means ± SD from three independent experiments. *, $P < 0.05$; **, $P < 0.01$; ***, $P < 0.001$ (two-tailed Student's *t*-test, compared with cells without co-expression of HRD1-myc).

(F) Cycloheximide-chase analysis of NHK degradation. HEK 293 cells co-transfected with NHK, HRD1-myc, and S-SEL1L were chased for the indicated period after addition of cycloheximide. The cell lysate was separated by 10% SDS-PAGE and analyzed by Western blotting. The signal intensity of NHK is quantified in the graph. Error bars indicate means ± SD from three independent experiments. *, $P < 0.05$; **, $P < 0.01$ (two-tailed Student's *t*-test, compared with

cells co-transfected with HRD1-myc).

Figure 6. Deletion of SEL1L proline-rich region promotes SEL1L degradation.

(A) Western blot analysis of HEK 293, HeLa, HepG2 (HG2), RD, and Capan2 cells (upper panel), and Coomassie Brilliant Blue (CBB) staining of the same membrane (lower panel). Twenty micrograms of each cell lysate was separated by SDS-PAGE and blotted with anti-SEL1L antibody.

(B) Cells were transfected with SEL1L-HA and treated with MG12 for 6 h (MG132 +). Arrows indicate full-length SEL1L-HA, and angle brackets denote SEL1L-HA degradation intermediates. Asterisks indicate non-specific signal detected by anti-HA antibody.

(C) Western blot analysis of SEL1L-HA and SEL1L-ΔPR-HA expressed in HEK 293 cells. Red arrow and angle brackets denote full-length SEL1L-ΔPR-HA and degradation intermediates, respectively.

(D) Pulse-chase analysis of NHK-QQQ and SEL1L-ΔPR-HA degradation. HEK 293 cells co-transfected with NHK-QQQ and SEL1L-HA or SEL1L-ΔPR-HA were metabolically labeled for 15 min and chased for the indicated period. Radioisotope incorporation into NHK-QQQ and SEL1L-HA or SEL1L-ΔPR-HA is quantified in the graph. Error bars indicate means ± SD from three independent experiments. *, $P < 0.05$; **, $P < 0.01$ (two-tailed Student's *t*-test).

Figure 7. Htt-polyQ76-GFP aggregates form in HEK293 cells.

(A) HEK 293 cells were transfected with Htt-polyQ76-GFP and SEL1L-HA or ΔssSEL1L-HA. Twenty-four hours after transfection, nuclei were stained with Hoechst 33342 and analyzed by fluorescence microscopy. MG132 was added 6 h prior to microscopic observation (MG132 +). Scale bars, 50 μm.

(B) Cells in A containing Htt-polyQ76-GFP aggregates were counted, and the percentage of GFP-positive cells (~300–500 cells) with aggregates was calculated. Error bars indicate means ± SD from three independent experiments. ns, $P > 0.05$; *, $P < 0.05$; **, $P < 0.01$; ***, $P < 0.001$ (two-tailed Student's *t*-test, compared with mock-transfected cells (MG132 -), or between the samples indicated by the bracket).

(C) Immunocytochemistry of HeLa cells transfected with SEL1L-HA or ΔssSEL1L-HA, treated with or without MG132. Cells were fixed and stained with anti-HA and anti-calreticulin (CRT, ER marker, left panel) or anti-HA and anti-HSP70/HSC70 (cytosolic marker) antibodies (right panel). SEL1L-HA and ΔssSEL1L-HA were visualized with Alexa Fluor 594, CRT and HSP70/HSC70 were stained with Alexa Fluor 488, and images were acquired by confocal microscopy. Scale bars, 10 μm.

Figure 8. Immunostaining of polyQ inclusions.

HEK 293 cells (A, B, C, E, and F) and HeLa cells (D) were transfected with Htt-polyQ76-GFP and SEL1L-HA (A, B and D), Htt-polyQ76-GFP and ΔssSEL1L-HA (C, D), Htt-polyQ23 and SEL1L-HA (E), or Htt-polyQ23 and ΔssSEL1L-HA (F). Twenty-four hours after transfection, cells were fixed and stained with anti-GFP and anti-HA antibodies. GFP was visualized with Alexa Fluor 488, HA was stained with Alexa Fluor 596, and images were analyzed by confocal microscopy. MG132 was added 6 h prior to microscopic observation (MG132 +). Nuclei were counterstained with DAPI. Scale bars, 10 μm (upper panel) and 5 μm (magnified).

Figure 9. SEL1L SLR expressed in the cytosol promotes polyQ aggregation.

(A, B) Htt-polyQ76-GFP aggregation formation analyzed by fluorescence microscopy. Same as in Fig. 7A and B, except that cells were co-transfected with SEL1L-R5-9-HA.

(C) Immunostaining of Htt-polyQ76-GFP. Same as in Fig. 8B, except that cells were co-transfected with SEL1L-R5-9-HA.

(D, E) Filter-trap assays of Htt-polyQ76-GFP co-transfected with SEL1L-HA, Htt-polyQ23-GFP (D), and Htt-polyQ76-GFP co-transfected with mock, ΔssSEL1L-HA, or SEL1L-R5-9-HA (E). Cell lysates were serially diluted, and the indicated amounts of protein were applied to the filter.

(F) Model of HRD1–SEL1L complex formation. SEL1L and HRD1 form a stable complex in the

ER membrane, but SEL1L expressed in excess is rapidly degraded by ERAD (left). OS-9 and XTP3-B associate with and stabilize SEL1L until the HRD1–SEL1L complex is formed. Alternatively, SEL1L–lectin complex surveils the ER for misfolded proteins and dynamically forms a HRD1-containing membrane complex that is competent for retrotranslocation (right).

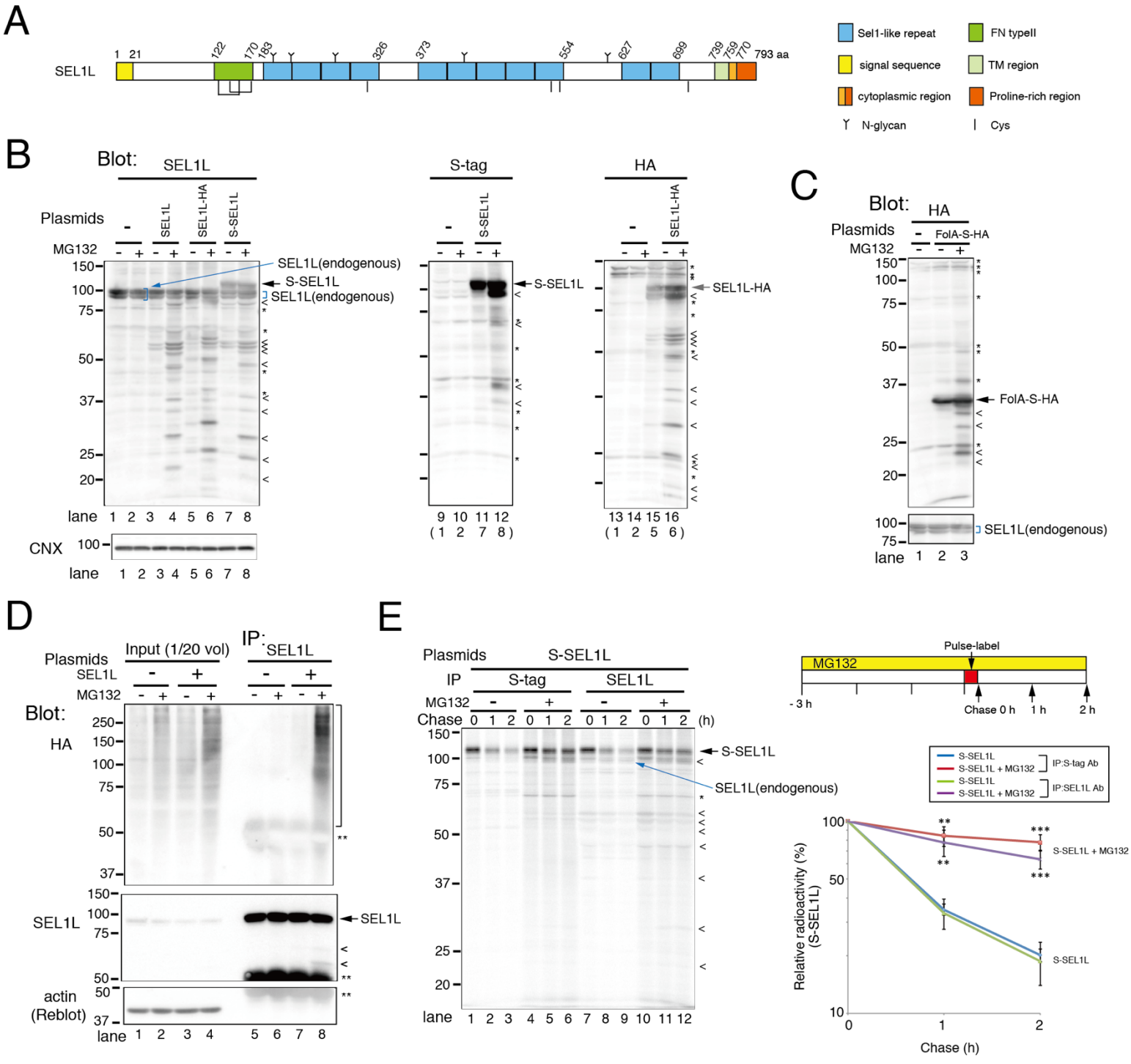
A
SEL1L
1 21 122 170 183 326 373 554 627 699 739 759 770 793 aa
Sel1-like repeat
FN typeII
signal sequence
TM region
cytoplasmic region
Proline-rich region
N-glycan
Cys
B
Blot: SEL1L
Plasmids
SEL1L
SEL1L-HA
S-SEL1L
MG132
SEL1L(endogenous)
S-SEL1L
SEL1L(endogenous)
lane 1 2 3 4 5 6 7 8
CNX
S-tag
S-SEL1L
9 10 11 12
(1 2 7 8)
HA
SEL1L-HA
13 14 15 16
(1 2 5 6)
C
Blot: HA
Plasmids
FolA-S-HA
MG132
FolA-S-HA
SEL1L(endogenous)
lane 1 2 3
D
Plasmids
Input (1/20 vol)
IP: SEL1L
SEL1L
MG132
Blot:
HA
SEL1L
actin
(Reblot)
lane 1 2 3 4 5 6 7 8
E
Plasmids
S-SEL1L
IP
S-tag
SEL1L
MG132
Chase 0 1 2 0 1 2 0 1 2 0 1 2 (h)
S-SEL1L
SEL1L(endogenous)
lane 1 2 3 4 5 6 7 8 9 10 11 12
Pulse-label
MG132
- 3 h
Chase 0 h
1 h
2 h
S-SEL1L
S-SEL1L + MG132
IP:S-tag Ab
S-SEL1L
S-SEL1L + MG132
IP:SEL1L Ab
Relative radioactivity (%)
(S-SEL1L)
S-SEL1L + MG132
S-SEL1L
Chase (h)

Figure 1

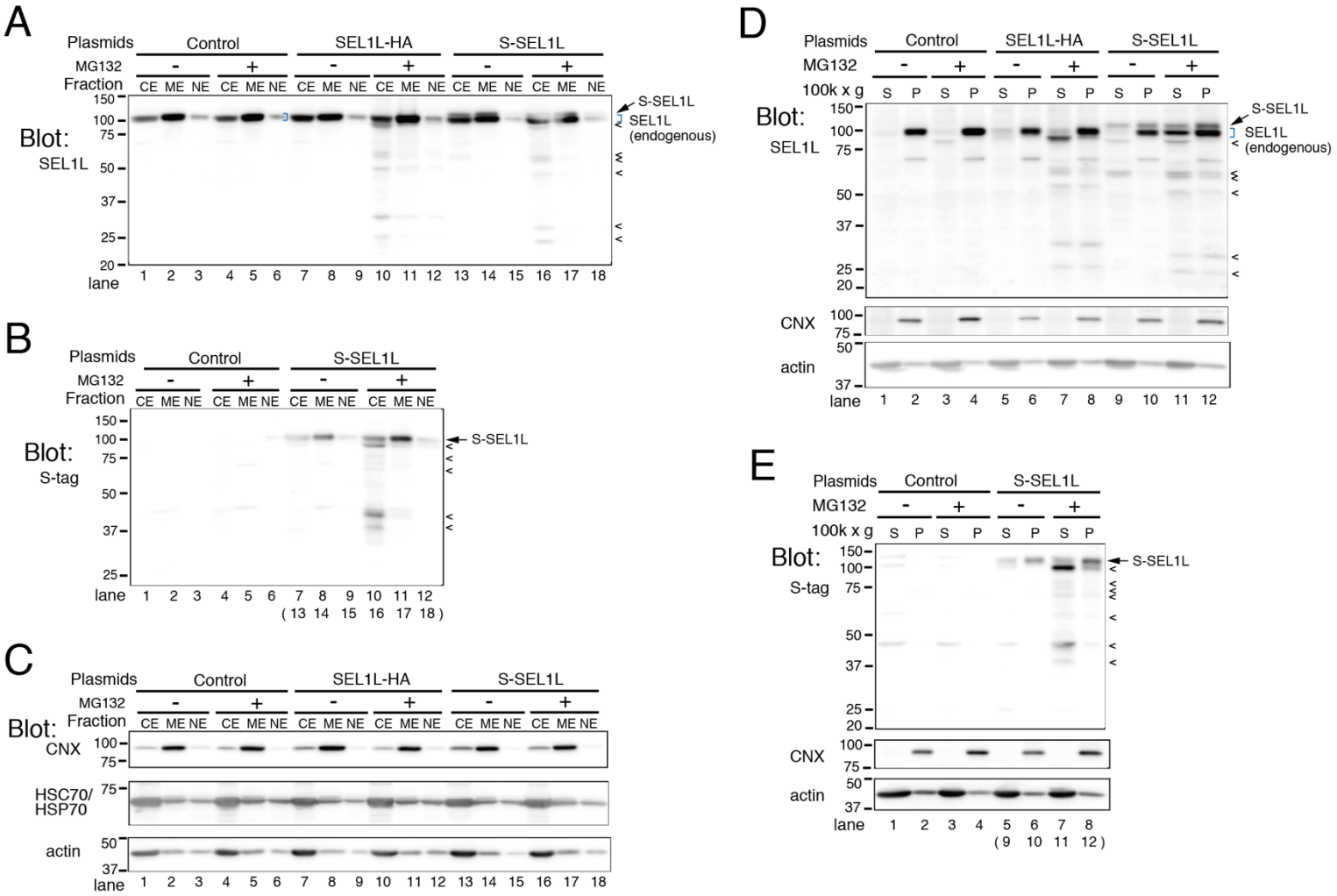
A
Plasmids
Control
SEL1L-HA
S-SEL1L
MG132
Fraction
CE ME NE
Blot:
SEL1L
S-SEL1L
SEL1L (endogenous)
lane
B
S-tag
C
CNX
HSC70/ HSP70
actin
D
100k x g
S P
E

Figure 2

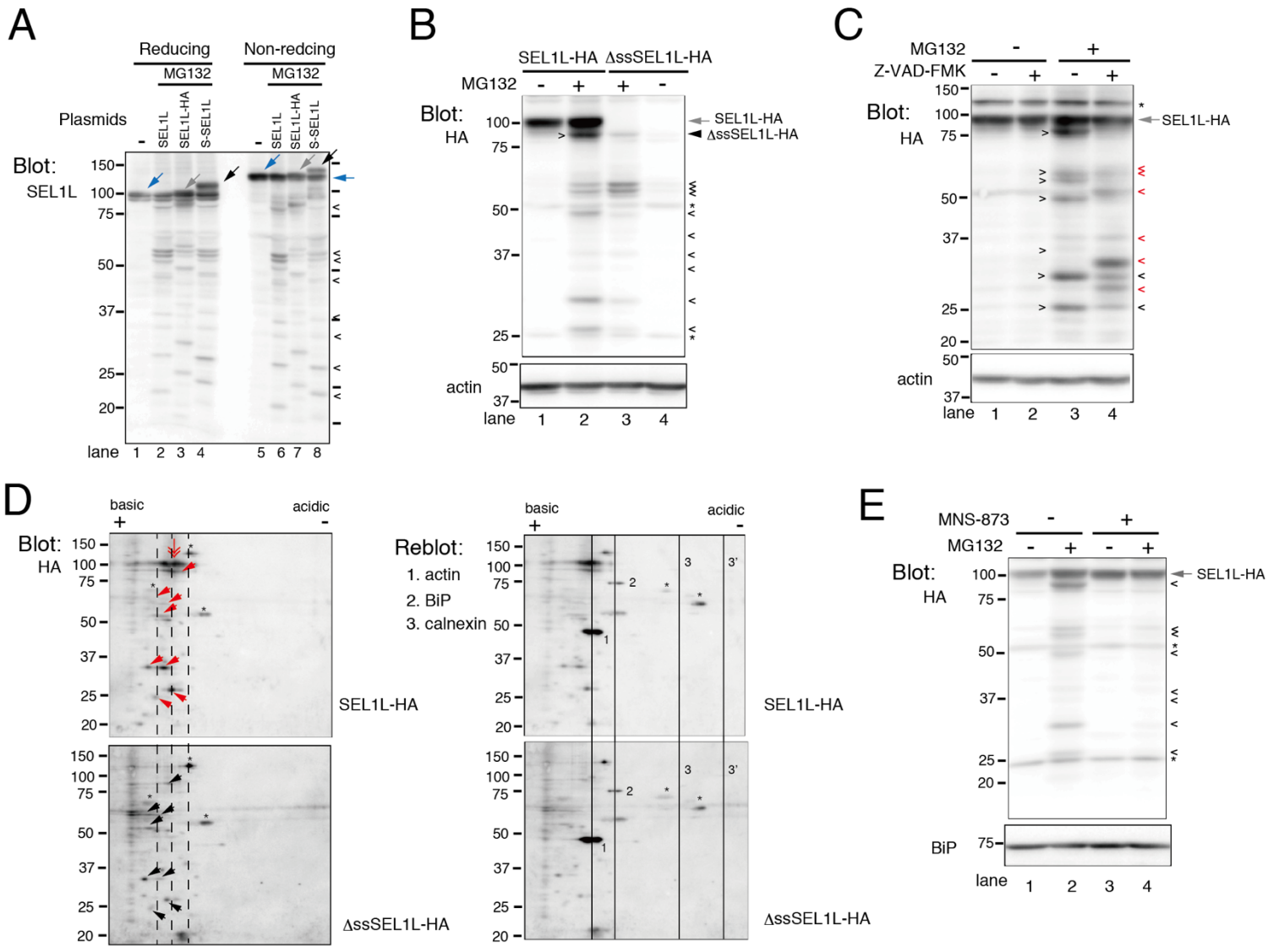
A
Reducing
Non-redcing
MG132
MG132
Plasmids
-
SEL1L
SEL1L-HA
S-SEL1L
-
SEL1L
SEL1L-HA
S-SEL1L
Blot:
SEL1L
150
100
75
50
37
25
20
lane 1 2 3 4 5 6 7 8
B
SEL1L-HA ΔssSEL1L-HA
MG132 - + + -
Blot:
HA
100
75
50
37
25
SEL1L-HA
ΔssSEL1L-HA
actin
50
37
lane 1 2 3 4
C
MG132 - +
Z-VAD-FMK - + - +
Blot:
HA
150
100
75
50
37
25
20
SEL1L-HA
actin
50
37
lane 1 2 3 4
D
basic
acidic
+
-
Blot:
HA
150
100
75
50
37
25
20
SEL1L-HA
ΔssSEL1L-HA
Reblot:
1. actin
2. BiP
3. calnexin
basic
acidic
+
-
1
2
3
3'
SEL1L-HA
ΔssSEL1L-HA
E
MNS-873 - +
MG132 - + - +
Blot:
HA
100
75
50
37
25
20
SEL1L-HA
BiP
75
lane 1 2 3 4

Figure 3

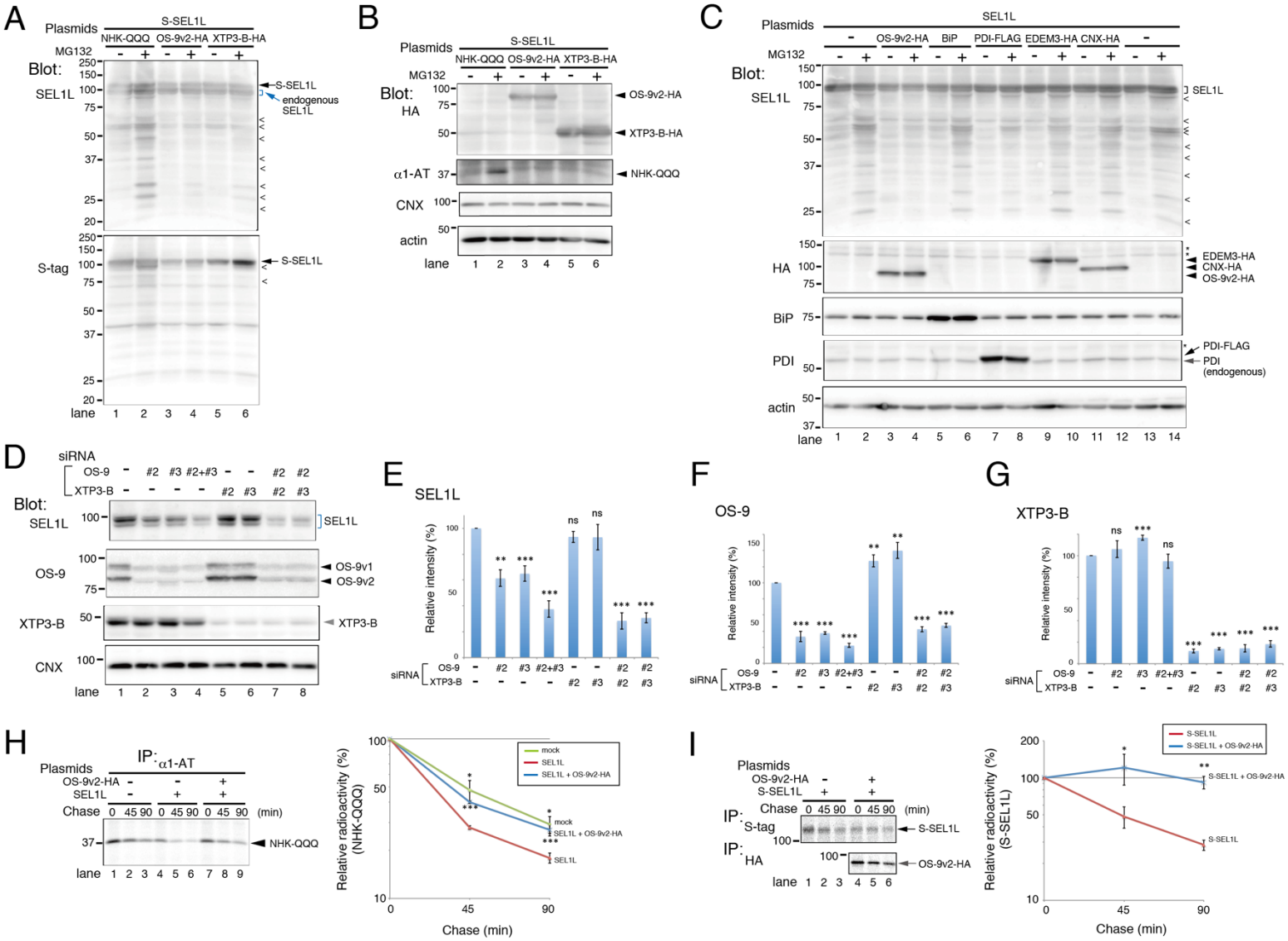
A
Plasmids
S-SEL1L
NHK-QQQ OS-9v2-HA XTP3-B-HA
MG132
Blot:
SEL1L
S-SEL1L
endogenous SEL1L
S-tag
S-SEL1L
lane 1 2 3 4 5 6
B
Plasmids
S-SEL1L
NHK-QQQ OS-9v2-HA XTP3-B-HA
MG132
Blot:
HA
OS-9v2-HA
XTP3-B-HA
α1-AT
NHK-QQQ
CNX
actin
lane 1 2 3 4 5 6
C
Plasmids
SEL1L
OS-9v2-HA BiP PDI-FLAG EDEM3-HA CNX-HA
MG132
Blot:
SEL1L
HA
EDEM3-HA
CNX-HA
OS-9v2-HA
BiP
PDI
PDI-FLAG
PDI (endogenous)
actin
lane 1 2 3 4 5 6 7 8 9 10 11 12 13 14
D
siRNA
OS-9
XTP3-B
Blot:
SEL1L
OS-9
OS-9v1
OS-9v2
XTP3-B
CNX
lane 1 2 3 4 5 6 7 8
E
SEL1L
Relative intensity (%)
siRNA
OS-9
XTP3-B
F
OS-9
Relative intensity (%)
siRNA
OS-9
XTP3-B
G
XTP3-B
Relative intensity (%)
siRNA
OS-9
XTP3-B
H
IP: α1-AT
Plasmids
OS-9v2-HA
SEL1L
Chase 0 45 90 0 45 90 0 45 90 (min)
NHK-QQQ
lane 1 2 3 4 5 6 7 8 9
Relative radioactivity (%) (NHK-QQQ)
mock
SEL1L
SEL1L + OS-9v2-HA
Chase (min)
I
Plasmids
OS-9v2-HA
S-SEL1L
Chase 0 45 90 0 45 90 (min)
IP: S-tag
S-SEL1L
IP: HA
OS-9v2-HA
lane 1 2 3 4 5 6
Relative radioactivity (%) (S-SEL1L)
S-SEL1L
S-SEL1L + OS-9v2-HA
Chase (min)

Figure 4

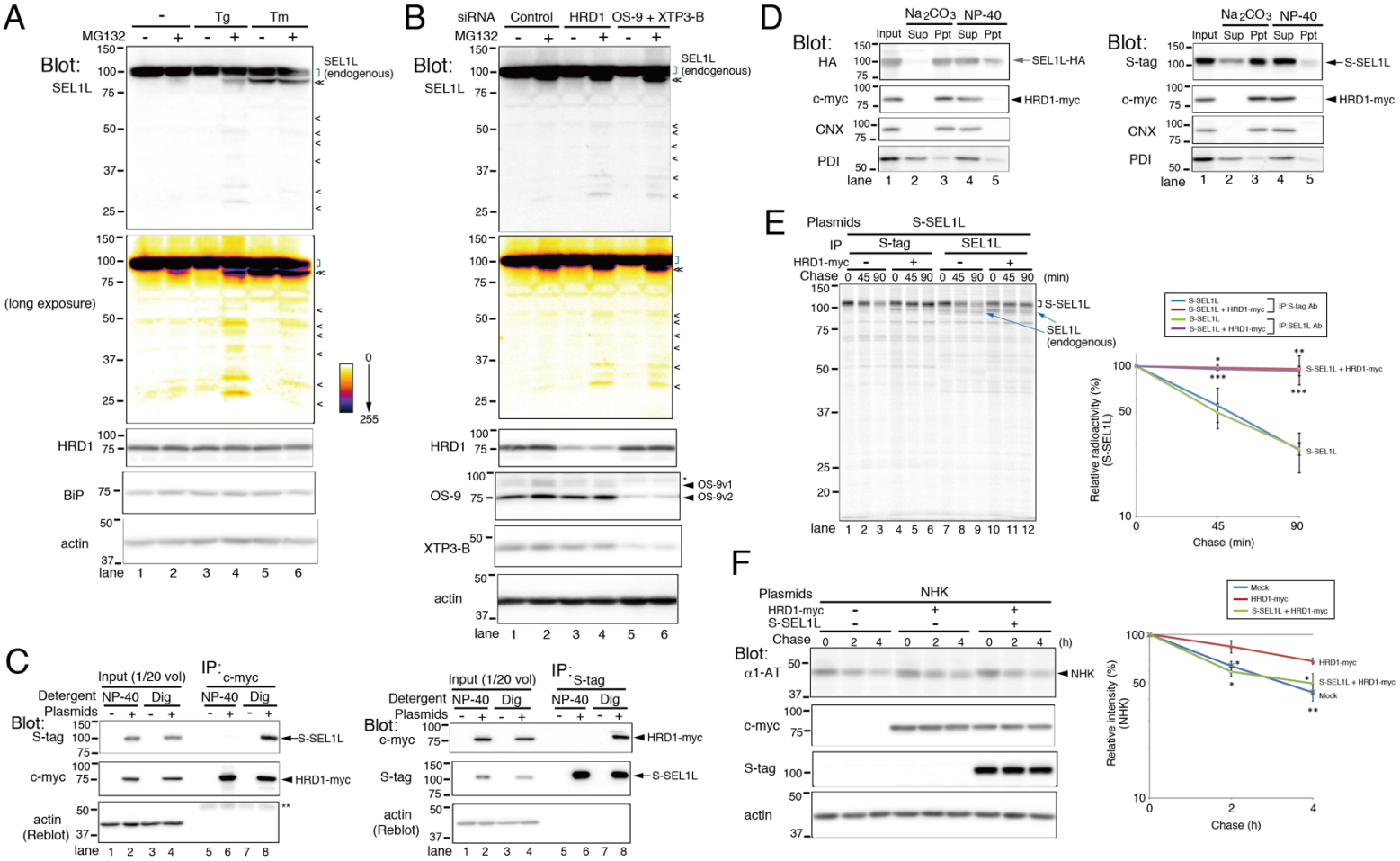
A
MG132
Tg
Tm
Blot:
SEL1L
(endogenous)
(long exposure)
HRD1
BiP
actin
lane
B
siRNA
Control
HRD1
OS-9 + XTP3-B
OS-9
XTP3-B
OS-9v1
OS-9v2
C
Input (1/20 vol)
IP: c-myc
IP: S-tag
Detergent
NP-40
Dig
Plasmids
S-tag
c-myc
S-SEL1L
HRD1-myc
actin
(Reblot)
D
Na2CO3
NP-40
Input
Sup
Ppt
HA
SEL1L-HA
CNX
PDI
E
Plasmids
S-SEL1L
IP
S-tag
SEL1L
HRD1-myc
Chase
(min)
Relative radioactivity (%)
(S-SEL1L)
Chase (min)
IP:S-tag Ab
IP:SEL1L Ab
F
NHK
α1-AT
Relative intensity (%)
(NHK)
Chase (h)
Mock

Figure 5

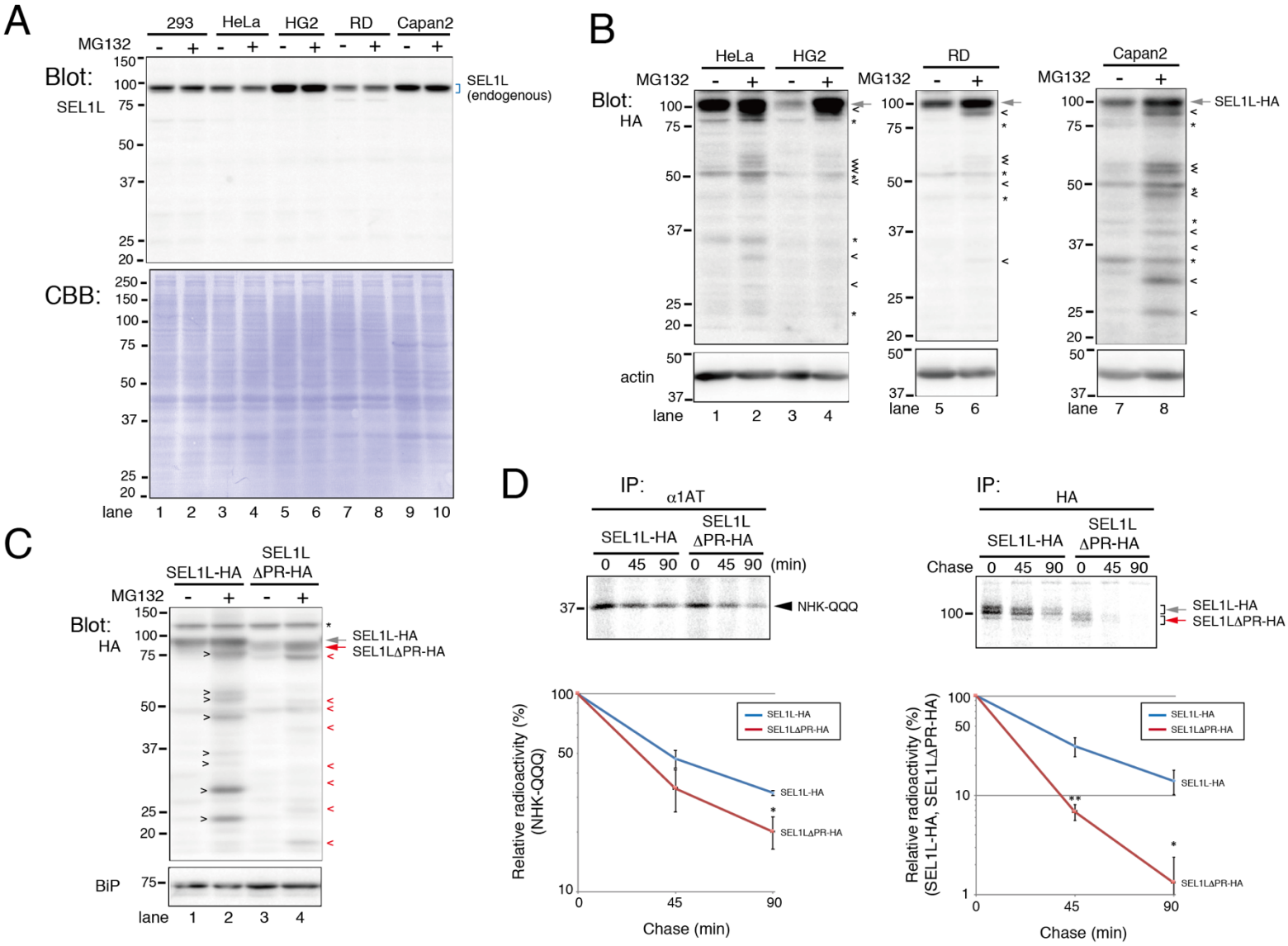
A
293
HeLa
HG2
RD
Capan2
MG132
Blot:
SEL1L
SEL1L (endogenous)
CBB:
lane
B
HeLa
HG2
RD
Capan2
MG132
Blot:
HA
SEL1L-HA
actin
lane
C
SEL1L-HA
SEL1L ΔPR-HA
MG132
Blot:
HA
SEL1L-HA
SEL1LΔPR-HA
BiP
lane
D
IP:
α1AT
SEL1L-HA
SEL1L ΔPR-HA
0 45 90 0 45 90 (min)
NHK-QQQ
IP:
HA
Chase 0 45 90 0 45 90
SEL1L-HA
SEL1LΔPR-HA
Relative radioactivity (%) (NHK-QQQ)
Chase (min)
Relative radioactivity (%) (SEL1L-HA, SEL1LΔPR-HA)
Chase (min)

Figure 6

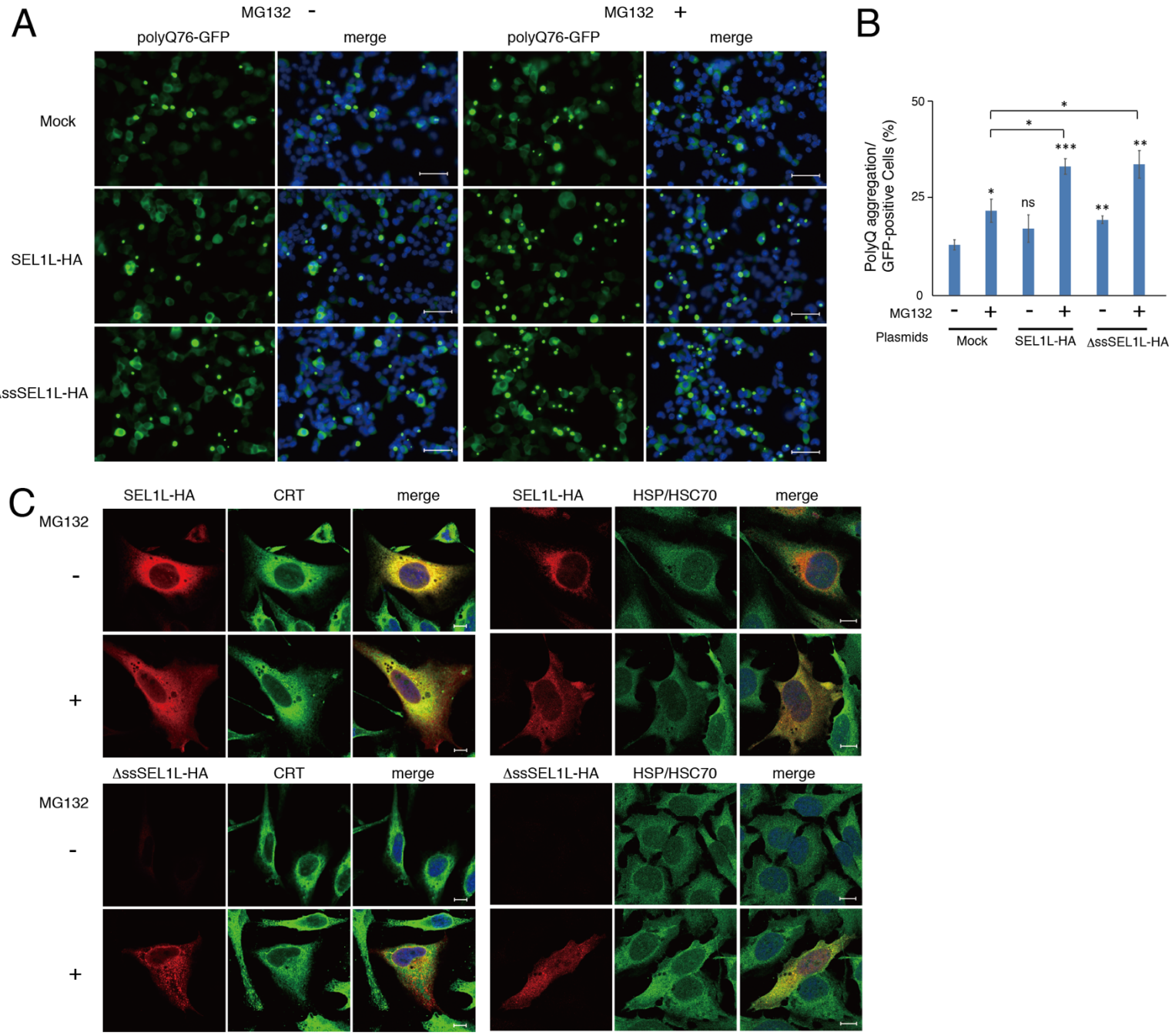
A
MG132 -
MG132 +
polyQ76-GFP
merge
polyQ76-GFP
merge
Mock
SEL1L-HA
ΔssSEL1L-HA
B
PolyQ aggregation/
GFP-positive Cells (%)
50
25
0
*
*
*
***
**
**
ns
MG132
- + - + - +
Plasmids
Mock
SEL1L-HA
ΔssSEL1L-HA
C
SEL1L-HA
CRT
merge
SEL1L-HA
HSP/HSC70
merge
MG132
-
+
ΔssSEL1L-HA
CRT
merge
ΔssSEL1L-HA
HSP/HSC70
merge
MG132
-
+

Figure 7

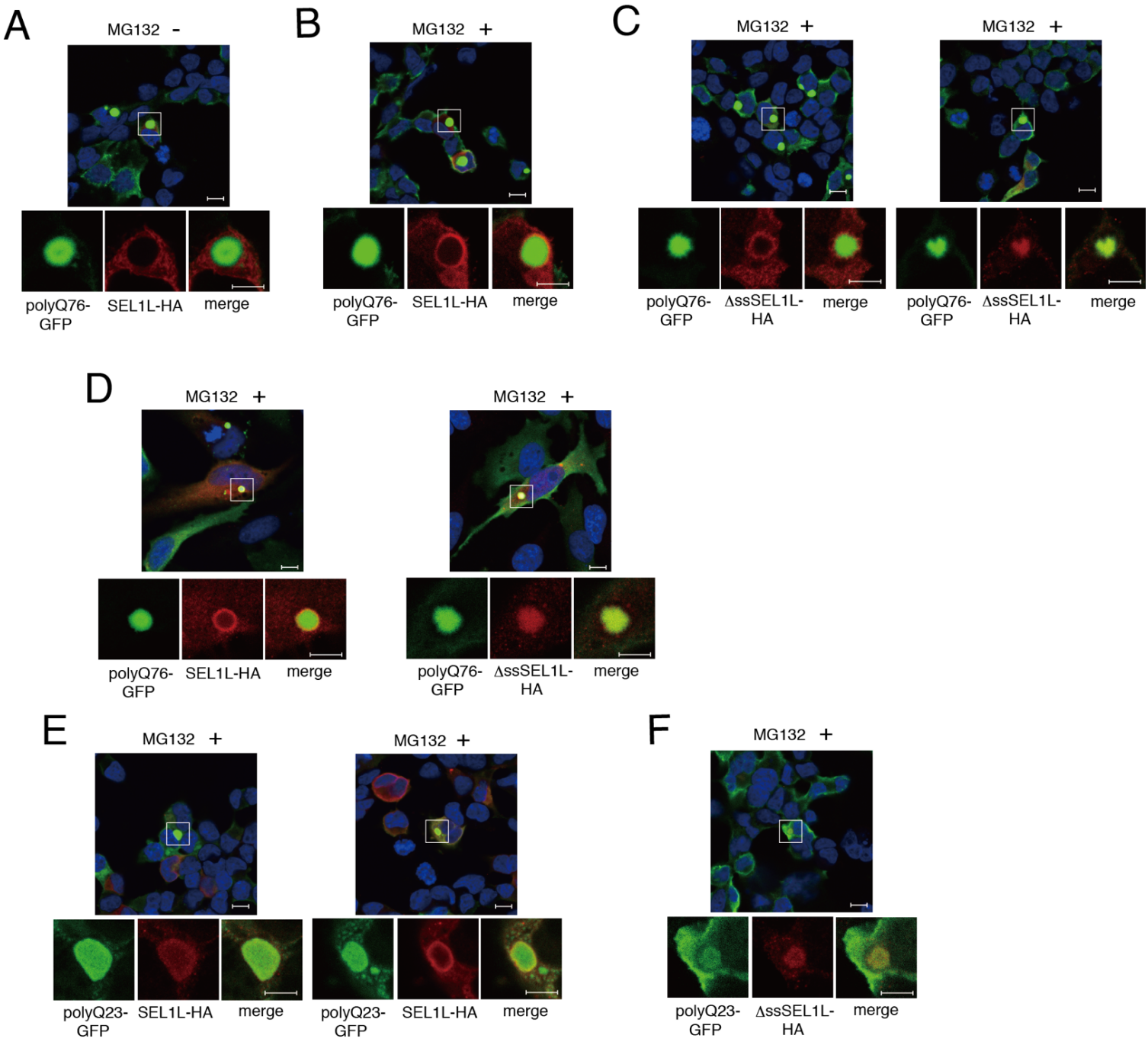
A
MG132 -
polyQ76-GFP
SEL1L-HA
merge
B
MG132 +
polyQ76-GFP
SEL1L-HA
merge
C
MG132 +
polyQ76-GFP
ΔssSEL1L-HA
merge
MG132 +
polyQ76-GFP
ΔssSEL1L-HA
merge
D
MG132 +
polyQ76-GFP
SEL1L-HA
merge
MG132 +
polyQ76-GFP
ΔssSEL1L-HA
merge
E
MG132 +
polyQ23-GFP
SEL1L-HA
merge
MG132 +
polyQ23-GFP
SEL1L-HA
merge
F
MG132 +
polyQ23-GFP
ΔssSEL1L-HA
merge

Figure 8

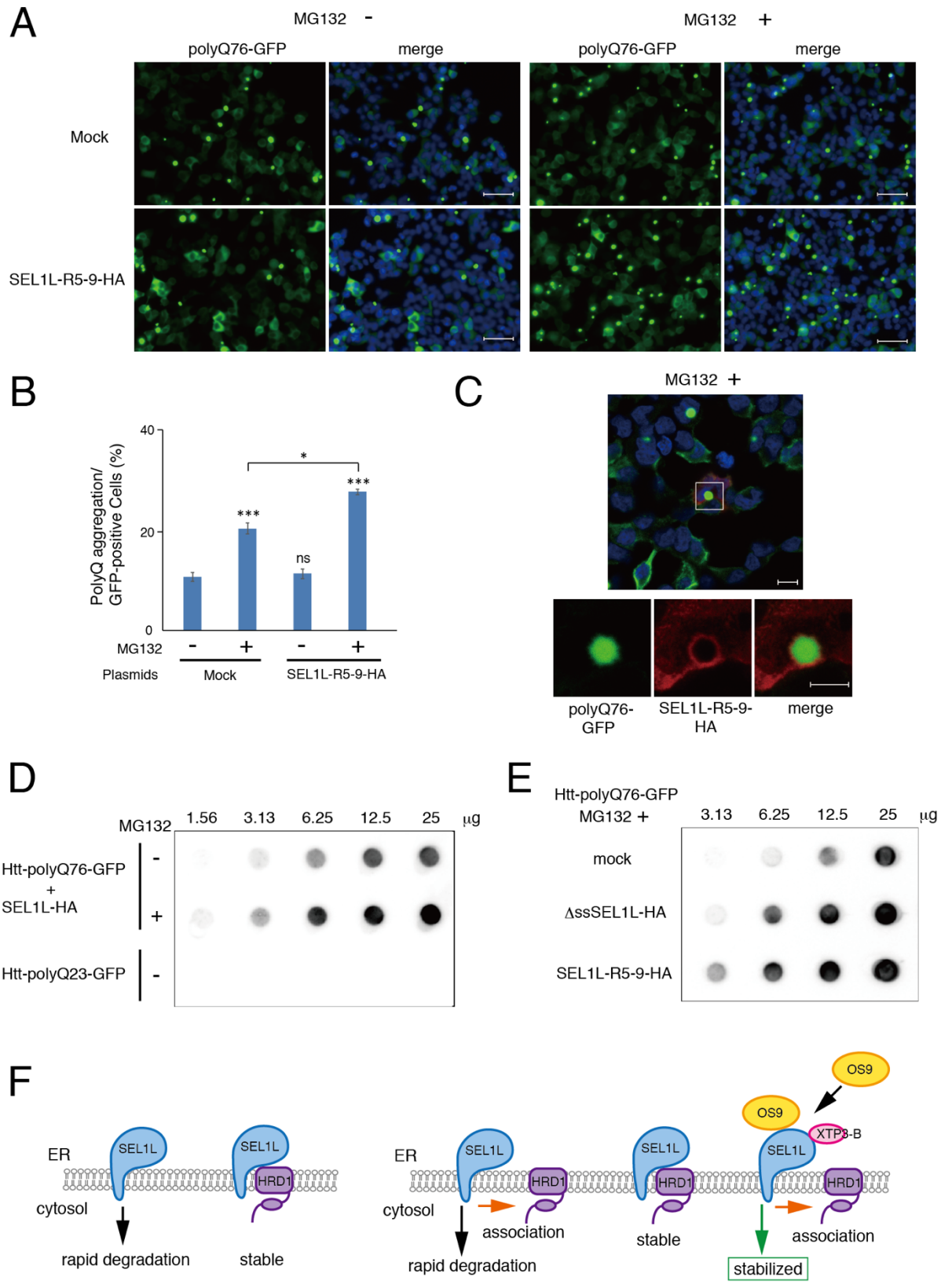
A
MG132 -
MG132 +
polyQ76-GFP
merge
polyQ76-GFP
merge
Mock
SEL1L-R5-9-HA
B
PolyQ aggregation/ GFP-positive Cells (%)
40
20
0
*
***
***
ns
MG132
-
+
-
+
Plasmids
Mock
SEL1L-R5-9-HA
C
MG132 +
polyQ76-GFP
SEL1L-R5-9-HA
merge
D
MG132
1.56
3.13
6.25
12.5
25
μg
Htt-polyQ76-GFP
+
SEL1L-HA
-
+
Htt-polyQ23-GFP
-
E
Htt-polyQ76-GFP
MG132 +
3.13
6.25
12.5
25
μg
mock
ΔssSEL1L-HA
SEL1L-R5-9-HA
F
ER
SEL1L
SEL1L
HRD1
cytosol
rapid degradation
stable
ER
SEL1L
HRD1
SEL1L
HRD1
OS9
OS9
XTP3-B
SEL1L
HRD1
cytosol
association
stable
association
rapid degradation
stabilized

Figure 9